

AD-A170 384

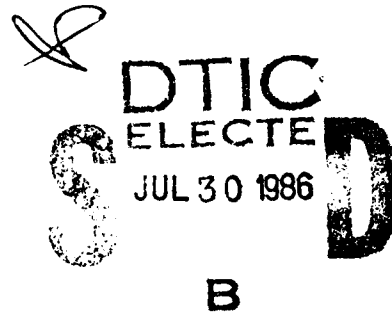
(1)

ARMC Report No. 4.76-1

ANALYSIS OF DUCTED PROPELLERS IN STEADY FLOW

R. Van Houten

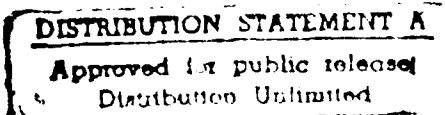
February, 1986



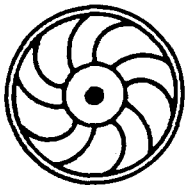
DTIC FILE COPY



AIRFLOW RESEARCH AND MANUFACTURING CORP.



86 7 20 072



AIRFLOW RESEARCH AND MANUFACTURING CORP.

304 Pleasant Street
Watertown, MA 02172
(617) 926-3061
Telex 294129 ARMC UR

ARMC Report No. 4.76-1

ANALYSIS OF DUCTED PROPELLERS IN STEADY FLOW

R. Van Houten

February, 1986

Copyright (c) Airflow Research and Manufacturing Corporation
and Massachusetts Institute of Technology, 1986.

This research was carried out under subcontract GC-A-483454 from
Massachusetts Institute of Technology (MIT OSP 94409)
in support of contract N00014-84-K-0072 under the
Naval Sea Systems Command
General Hydromechanics Research (GHR) Program
administered by the
David W. Taylor Naval Ship Research and Development Center

APPROVED FOR PUBLIC RELEASE
DISTRIBUTION UNLIMITED

JUL 30 1986

B

UNCLASSIFIED

SECURITY CLASSIFICATION OF THIS PAGE

AD-A176 384

REPORT DOCUMENTATION PAGE

1a REPORT SECURITY CLASSIFICATION UNCLASSIFIED		1b RESTRICTIVE MARKINGS N/A	
2a SECURITY CLASSIFICATION AUTHORITY N/A		3 DISTRIBUTION/AVAILABILITY OF REPORT APPROVED FOR PUBLIC RELEASE; DISTRIBUTION UNLIMITED	
2b DECLASSIFICATION/DOWNGRADING SCHEDULE N/A		5 MONITORING ORGANIZATION REPORT NUMBER(S)	
4 PERFORMING ORGANIZATION REPORT NUMBER(S) ARMC 4.76-1		6a NAME OF PERFORMING ORGANIZATION Airflow Research & Manufacturing Corp.	
6b OFFICE SYMBOL (If applicable)		7a NAME OF MONITORING ORGANIZATION DAVID W. TAYLOR NAVAL SHIP RESEARCH AND DEVELOPMENT CENTER, Code 1504 (1505)	
6c ADDRESS (City, State, and ZIP Code) 304 Pleasant St. Watertown, MA 02172		7b ADDRESS (City, State, and ZIP Code) BETHESDA, MARYLAND 20084-5000	
8a NAME OF FUNDING/SPONSORING ORGANIZATION Naval Sea Systems Command		8b OFFICE SYMBOL (If applicable) SEA 05R24	
8c ADDRESS (City, State, and ZIP Code) Washington, D. C. 20360		9 PROCUREMENT INSTRUMENT IDENTIFICATION NUMBER Contract Number - N00014-84-K-0072	
10 SOURCE OF FUNDING NUMBERS PROGRAM ELEMENT NO 61153N		PROJECT NO SR 023 01	TASK NO 23454
11 TITLE (Include Security Classification) ANALYSIS OF DUCTED PROPELLERS IN STEADY FLOW. (Unclassified)		WORK UNIT ACCESSION NO N/A	
12 PERSONAL AUTHOR(S) R. Van Houten		13a TYPE OF REPORT Final	
13b TIME COVERED FROM 1/84 TO 2/86		14 DATE OF REPORT (Year Month Day) February 1986	
15 PAGE COUNT 61		16 SUPPLEMENTARY NOTATION Sponsored under the Naval Sea Systems Command General Hydromechanics Research (GHR) Program administered by the David W. Taylor Naval Ship R&D Center, Code 1504 (1505). Bethesda, Maryland 20084-5000	
17 COSATI CODES FIELD GROUP SUB-GROUP 20 04		18 SUBJECT TERMS (Continue on reverse if necessary and identify by block number) GHR Program, Propellers, Ducted Propellers, Tip Gap, Banded Propellers, Lifting Surface Theory, Vortex Lattice	
19 ABSTRACT (Continue on reverse if necessary and identify by block number) This report describes a computer program (DPSF); based on lifting surface theory, which analyzes the hydrodynamic performance of a ducted or banded propeller in an axisymmetric inflow. Special attention is given the modelling of flow through the clearance gap. Calculated results are compared with experimental data, and numerical convergence is demonstrated.		20 DISTRIBUTION/AVAILABILITY OF ABSTRACT <input checked="" type="checkbox"/> UNCLASSIFIED/UNLIMITED <input type="checkbox"/> SAME AS RPT <input type="checkbox"/> DTIC USERS	
21 ABSTRACT SECURITY CLASSIFICATION UNCLASSIFIED		22b TELEPHONE (Include Area Code) 202-227-1503	
22c OFFICE SYMBOL Code 1504/1505		23 APR edition may be used until exhausted All other editions are obsolete	

TABLE OF CONTENTS

1. BACKGROUND.	1
2. VISCOUS EFFECTS IN TIP GAP FLOWS.	4
3. LIFTING LINE REPRESENTATIONS OF FLOWS WITH TIP GAPS.	12
4. VORTEX LATTICE REPRESENTATION OF FLOWS WITH TIP GAPS.	25
5. THE DUCTED PROPELLER ANALYSIS PROGRAM.	29
Blade Geometry	30
Duct Geometry	32
Vortex Lattice	32
Wake Geometry	38
Wake Alignment	39
Source Strength	40
Solution of Boundary Value Problem	40
Force Calculation	41
Results	42
Computation Time	54
6. CONCLUSIONS AND RECOMMENDATIONS.	55
7. REFERENCES.	58
APPENDIX A - MAGNITUDE OF THE GAP BOUNDARY LAYER THICKNESS.	60

A-1

1. BACKGROUND

It has been known for some time that by operating a marine propeller in a duct (also called a shroud or nozzle), certain advantages can be obtained over an open propeller. When the duct is designed to accelerate the fluid through the propeller disk, the advantages include an increased ideal efficiency at a given propeller diameter, an efficiency curve which is fairly flat over a wide range of advance ratios, and high bollard pull. The disadvantages of the ducted propeller are that there is additional viscous drag on the duct surface, and cavitation can be a problem in the clearance gap between the blade tips and the duct. A propulsor which avoids the latter problem is the banded, or ring, propeller. In this configuration the shroud is attached to the blade tips, and rotates with the propeller. Viscous drag on the band contributes to shaft torque, resulting in a loss of efficiency, but high tip loading on the blades can be better maintained in the absence of a tip gap, and a concentrated tip vortex can be avoided in favor of a distributed vortex sheet in the wake of the band. This may result in delayed cavitation inception relative to an open propeller.

Ducted and banded propellers have been fitted mainly to ships operating at low speeds, with heavy disk loading, and particularly those which must operate at the zero speed condition, such as tugs and trawlers. However, recent attention has focused on these configurations for higher speed naval applications. In order to evaluate the suitability of ducted and banded propellers for these new applications, design and analysis methods must be developed for them.

A first step in this direction was taken when an analysis program for banded propellers was developed by Van Houten (1983) under the sponsorship of NSRDC. This program, called BPSF (Banded Propeller in Steady Flow), was an extension of PSF, a lifting surface analysis program for open propellers (Greeley, 1982; Greeley and Kerwin, 1982). In BPSF the radius of the band and its section characteristics (camber, thickness, and angle of attack) were allowed to vary circumferentially, the only restriction being that the axial extent of the band be equal to that of the tip of the blade. The objective of the work presented here was to develop an equivalent program for the analysis of ducted propellers.

This program, called DPSF, allows there to be an arbitrary tip gap between the propeller tip and the surface of the duct. The duct is constrained to be axisymmetric, but is allowed to extend axially well beyond the blade tip. This report presents some of the theory behind this program, and some representative results. Little effort will be made to recap the development of PSF and BPSF, for which the reader is referred to the beforementioned publications.

2. VISCOUS EFFECTS IN TIP GAP FLOWS

One of the fundamental problems to be faced in developing an analysis program for ducted propellers is the question of accurately modeling the clearance gap between the blade tip and the duct surface. This gap is typically a fraction of a percent of the propeller diameter, and the question arises as to the importance of viscous effects in determining the leakage flow. This question has been addressed in the past by several investigators, who have concluded in general that the leakage flow is largely inviscid in nature. This is supported by some simple scaling arguments outlined in Appendix A. Furthermore, the leakage volume flow rate is to a large extent independent of the chordwise flow. As a result simple two dimensional experiments can be used to investigate the flow in the clearance gap.

Such experiments have been carried out in the past by Shalnev (1954), Gearhart (1966), Booth, Dodge and Hepworth (1981), and Wadia and Booth (1981). The type of leakage flow they have found, in the case of a blade tip with a square cross-section, is shown in figure 2.1. The sharp corner at the entrance to the gap causes a separation bubble which then reattaches to the blade tip. The jet at the exit from the gap causes the rolling up of a vortex on the suction side of the blade. The presence of the separation

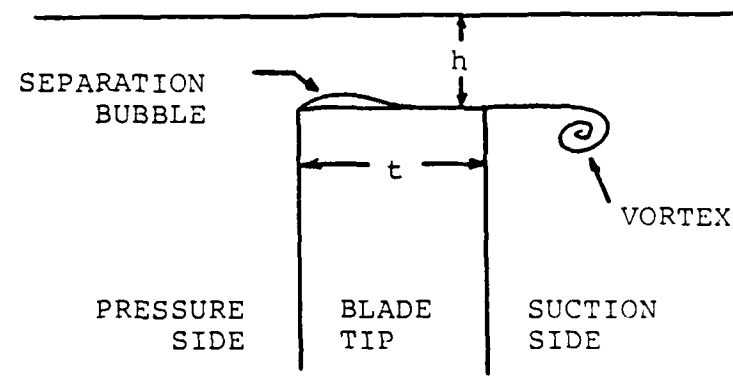


Figure 2.1 Observed flow past square blade tip.

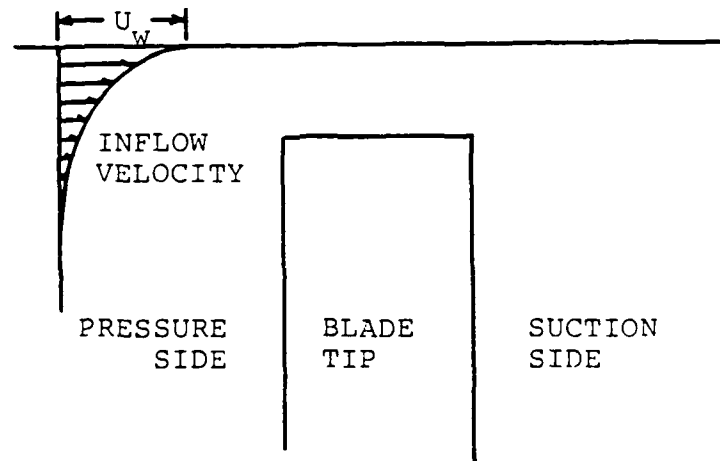


Figure 2.2 Inflow velocity distribution due to duct boundary layer.

bubble causes the total flow through the gap to be less than would otherwise be predicted. The reduction in flow is often given in terms of a discharge coefficient, defined as:

$$C_Q = \frac{Q}{\sqrt{2 \Delta p / \rho h}}$$

where Q = total volume flow through the gap

Δp = pressure difference across the gap

ρ = fluid density

h = clearance height

This coefficient is a strong function of blade tip shape. In the interest of reducing the pressure reduction which takes place at the gap entrance, and thereby delaying the onset of gap cavitation, the pressure side of the blade tip is often rounded off. This can eliminate flow separation in the gap, and results in an increase in C_Q . In this respect the goals of efficiency and good cavitation performance operate at cross purposes.

C_Q is also a function of the boundary layer on the surface of the duct. This boundary layer causes the relative inflow velocity vector to twist suddenly, becoming tangential at the duct surface. When this velocity vector is decomposed into chordwise and normal components, both components exhibit boundary layer characteristics. The normal velocity field, when viewed relative to the blade

tip, appears as shown in figure 2.2. This shear flow can be characterized in terms of the relative magnitude of the wall velocity U_w compared to the "ideal" leakage velocity:

$$U_w^* = \frac{U_w}{\sqrt{2 \Delta p / \rho}}$$

and the ratio of the displacement thickness to the clearance height (δ^* / h) . The effect of relative wall motion on the flow through the gap is two-fold: 1) For a given size separation bubble, the net leakage will be increased by the existance of the shear flow. 2) It has been observed experimentally by Gearhart (1966) and analytically by Wadia and Booth (1981) that the size of the separation bubble is decreased by the existance of the shear flow, thereby further increasing the total leakage flow.

Another parameter affecting the leakage flow is the thickness of the blade tip relative to the clearance height (t/h) . For the square blade tip, with or without a rounded entrance corner, this parameter appears not to have a strong effect, since the pressure is not changing significantly over the constant height region of the gap. The Reynolds number of the flow will also have some importance, both in determining the nature of the inflow boundary layer and in determining the size of the separation region.

Addressing for the sake of simplicity the cases of a square blade tip, with and without a rounded leading edge, with $U_w^* = 0$, table 2.1 gives the values for C_Q found by various investigators. Although the data is limited, it indicates that C_Q is relatively independent of both t/h and Reynolds number.

Of the investigators mentioned above, only Gearhart (1966) and Wadia and Booth (1981) investigated the effect of wall motion on the leakage flow. Wadia and Booth did so using a numerical model and considered only the case of a turbine, where the shear velocities oppose those due to the pressure gradient. Gearhart investigated a range of values of U_w^* , but presented C_Q values for $\delta^*/h \approx .20$ only. These are shown in figure 2.3. It can be seen that the curves approach one another at the higher values of U_w^* , indicating that the separated zone on the square blade tip may be eliminated under these conditions. The numerical results of Wadia and Booth for a square tip at $U_w^* = -1$ is also shown, although they do not indicate the displacement thickness of the boundary layer assumed. More data on the effect of wall motion, and in particular the effect of boundary layer thickness, would be very useful.

<u>Author</u>	<u>Reynolds Number</u>	<u>t/h</u>	<u>C_Q</u>
Square Tip:			
Shalnev	15000- 110000	5-30	.762-.838
Gearhart	270000	14	.82
Wadia, Booth	6500	6.3	.851
Booth, Dodge, Hepworth	2800	3.8-7.5	.80-.82
Rounded Entrance:			
Shalnev	39000- 115000	5-10	.884-.975
Gearhart	270000	14	.92

Table 2.1 Summary of experimental data on discharge coefficient for 2-D tip gap, with no wall motion.

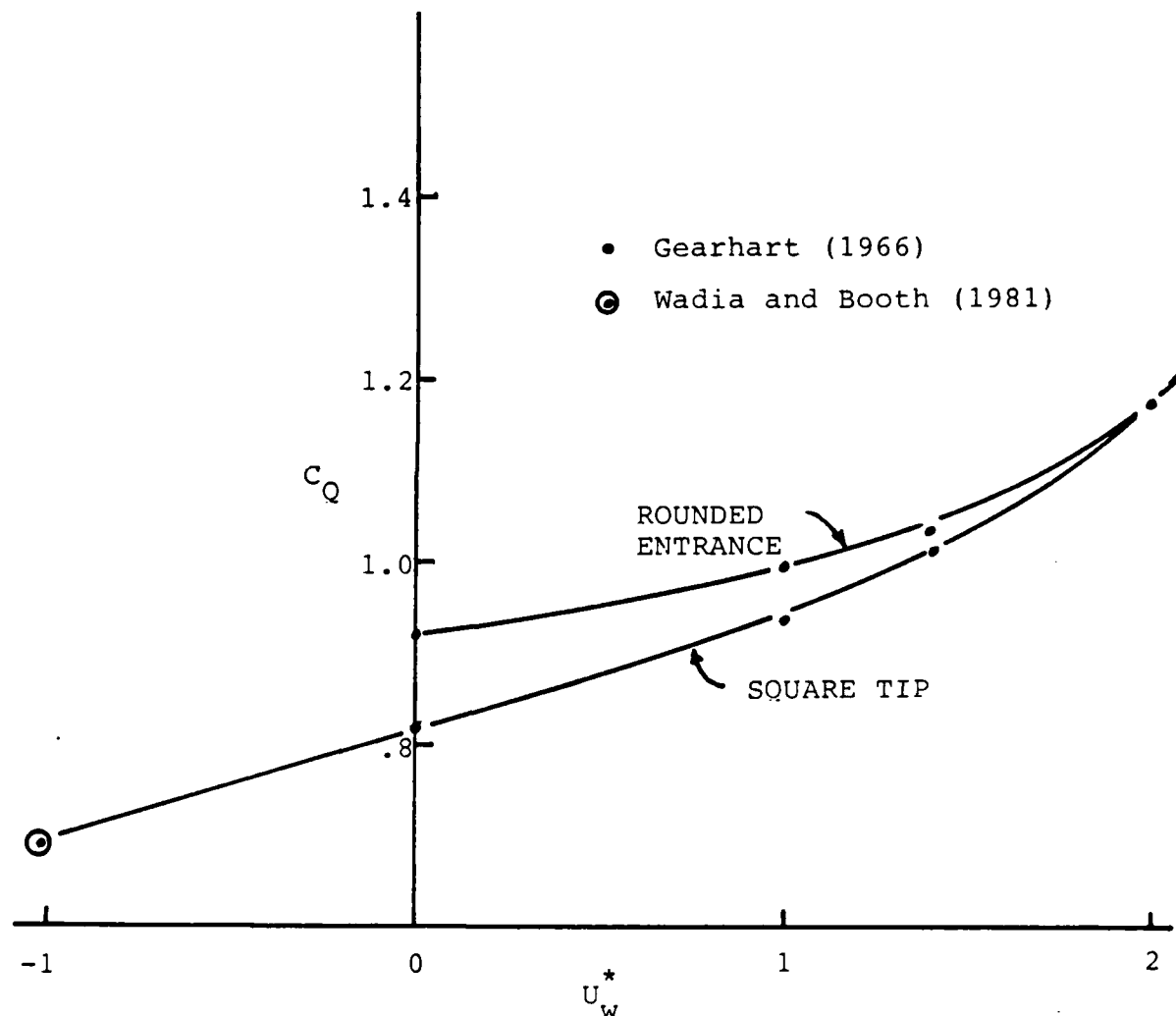


Figure 2.3 Effect of wall motion on discharge coefficient.

The application of data such as that shown in figure 2.3 to a global propeller analysis method is straightforward. It can be presumed that due to the very large mismatch in length scales between the clearance gap and the other propeller dimensions, the major impact of the clearance gap on the global flow field is the resulting leakage flow volume. Since C_Q represents the reduction in leakage volume due to viscous effects, these effects can be incorporated in the global flow field by using for analysis purposes an "inviscid" clearance gap height h_i equal to the product of C_Q and the physical gap height h :

$$h_i = C_Q \cdot h$$

3. LIFTING LINE REPRESENTATIONS OF FLOWS WITH TIP GAPS

The mismatch in length scales between the tip clearance height and the other relevant propeller dimensions makes difficult the development of a lifting surface theory for ducted propellers. In order to describe the small scale tip clearance region accurately one would normally have to use a vortex lattice whose spacing is small compared to the gap size, at least in the tip region. The total number of control points would be very large and the cost of running the program correspondingly high. In order to avoid this expense, a different approach was taken -- namely to determine if there is an optimum position of the outermost chordwise vortex on the blade such that numerical convergence can be accelerated. In order to find such an optimum, some numerical experiments were carried out using lifting line theory, with the supposition that the optimum spanwise arrangement of trailing vortices would not be affected by the chordwise arrangement of bound vorticities.

The initial configuration investigated was that of a straight lifting line normal to an infinite wall, and separated from that wall by a small gap. The effect of the wall was modeled by an image lifting line an equal distance on the other side of the wall. The circulation around the lifting line was represented by discrete horseshoe vortices. Figure 3.1 shows the arrangement of vortices and control

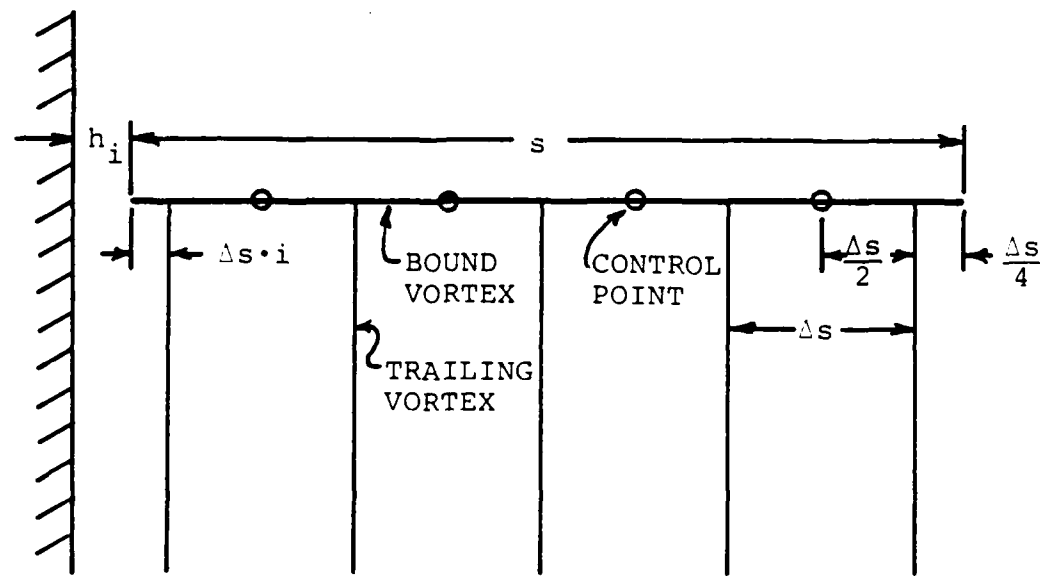


Figure 3.1 Lifting line representation of foil in presence of infinite wall -- linear spacing.

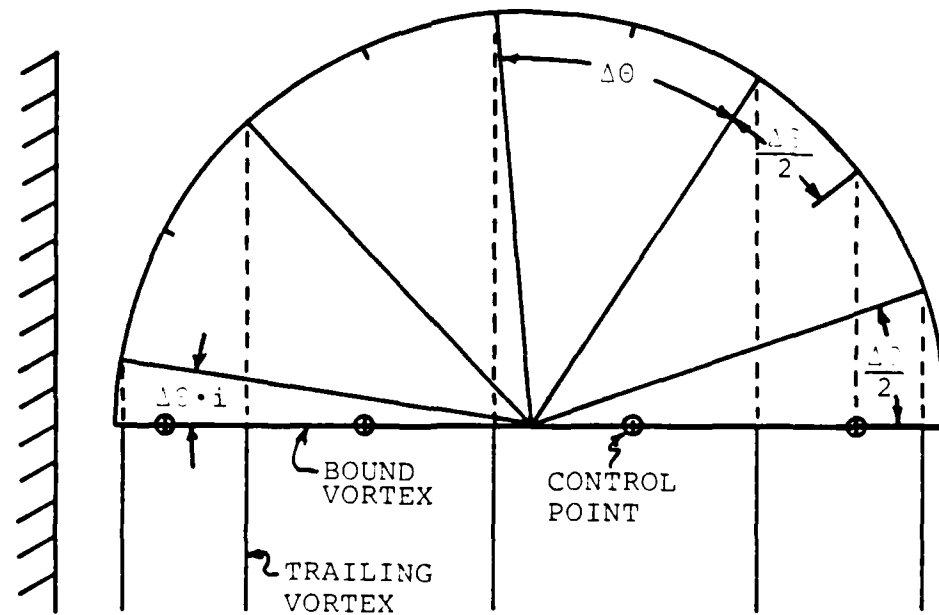


Figure 3.2 Lifting line representation of foil in presence of infinite wall -- cosine spacing.

points in the case of equally spaced trailers (linear spacing). The outermost trailers are inset from the tips of the foil by a fraction of the trailer spacing Δs . At the foil tip furthest from the wall, this inset fraction is taken to be .25. This is the inset normally used in the case of an isolated foil, and is analogous to the vortex position in 2-D vortex lattice theory (James, 1972). The optimum inset fraction "i" on the end near the wall is presumably not equal to .25, but approaches that value as the gap becomes large. For arbitrarily small gaps, the inset must approach zero, since in that case one would want to reproduce the results of a single foil of twice the aspect ratio. The problem can therefore be reduced to that of finding how the optimum inset fraction varies from zero to .25 as the gap varies from zero to infinity.

An alternative lifting line representation uses "cosine" spacing, with the discrete vortices and control points at equally spaced values of the Glauert angle θ as shown in figure 3.2. The inset fraction is defined as a fraction of the angular spacing $\Delta \theta$ of the vortices. On the free end this inset fraction is taken to be .5. This corresponds to common practice for isolated airfoils (Lan, 1974). At the end near the wall, the optimum inset fraction "i" must vary from zero to .5 as the gap is varied from zero to infinity.

In order to determine the optimum insets, numerical experiments were carried out. These experiments were performed on a foil with optimum loading, in the sense that induced drag is a minimum for a given lift. The "exact" circulation distribution was found for this case by using a large number of vortices (up to 400) with cosine spacing, and requiring the downwash to be a constant at all control points. The solution was then repeated, using a small number of vortices, and the inset was varied until a solution was obtained with the smallest mean-squared error between the calculated vortex strengths and the "exact" solution at the corresponding control points.

The results of these calculations are shown in figures 3.3 through 3.7. Figure 3.3 shows the calculated "exact" solution for an isolated foil (infinite gap) and gaps of .1, .01, .001, and .0001 of the span. In addition, the solutions are shown using optimum insets and linear spacing for 5, 10, and 20 vortices. It is clear that the use of an optimum inset results in a solution which is very close to the exact one, even when using very few vortices. Figure 3.4 shows comparable results for cosine spacing.

Figures 3.5 and 3.6 show the log of the optimum vortex inset fraction "i" plotted against the log of the ratio of gap width to the width of the last panel on the foil. It can be seen that when plotted in this way all the optimum

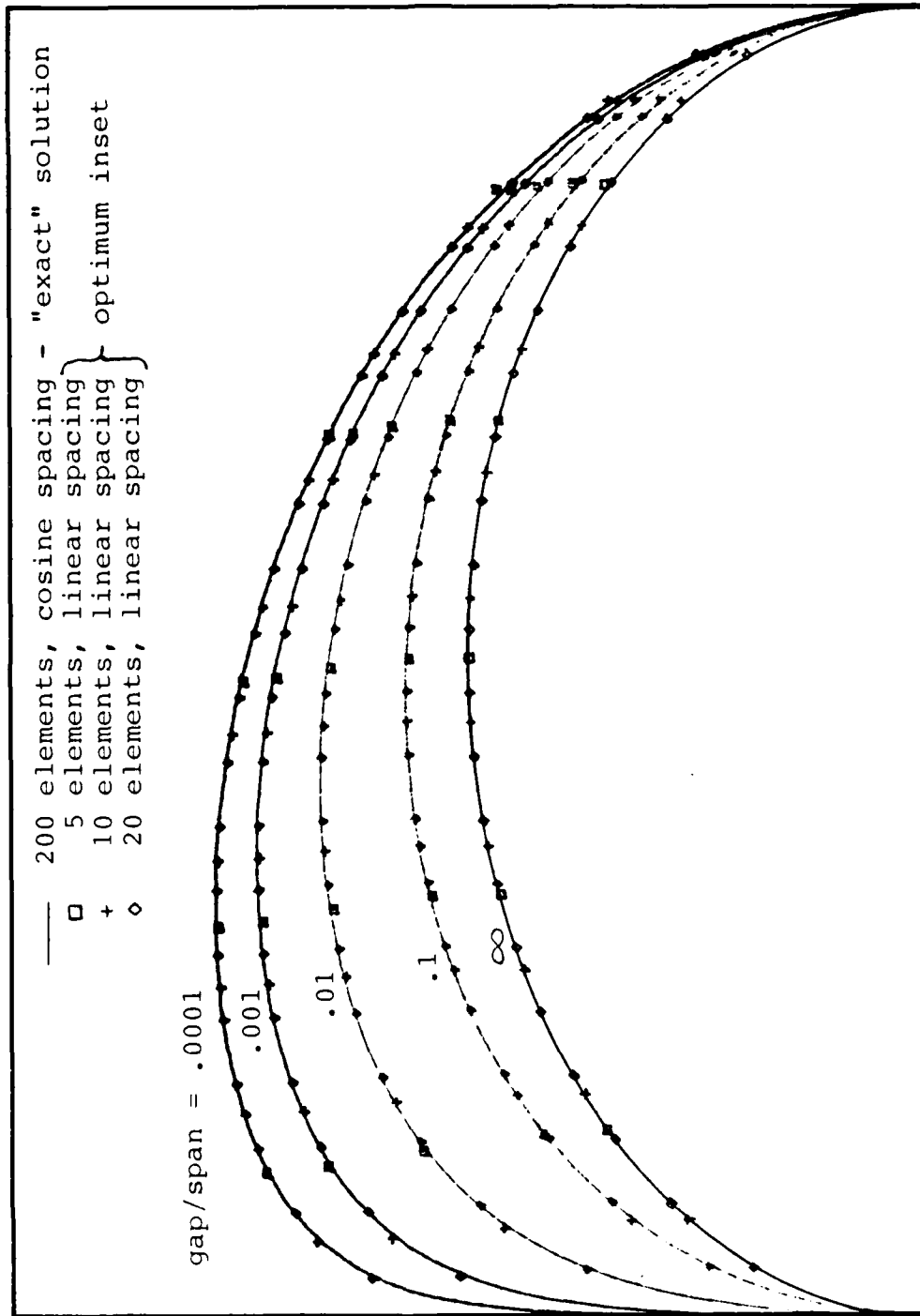


Figure 3.3 Circulation distribution on optimally loaded lifting line normal to wall, at various gap ratios. Comparison of "exact" solution with optimum 5, 10, and 20 element solutions, linear spacing.

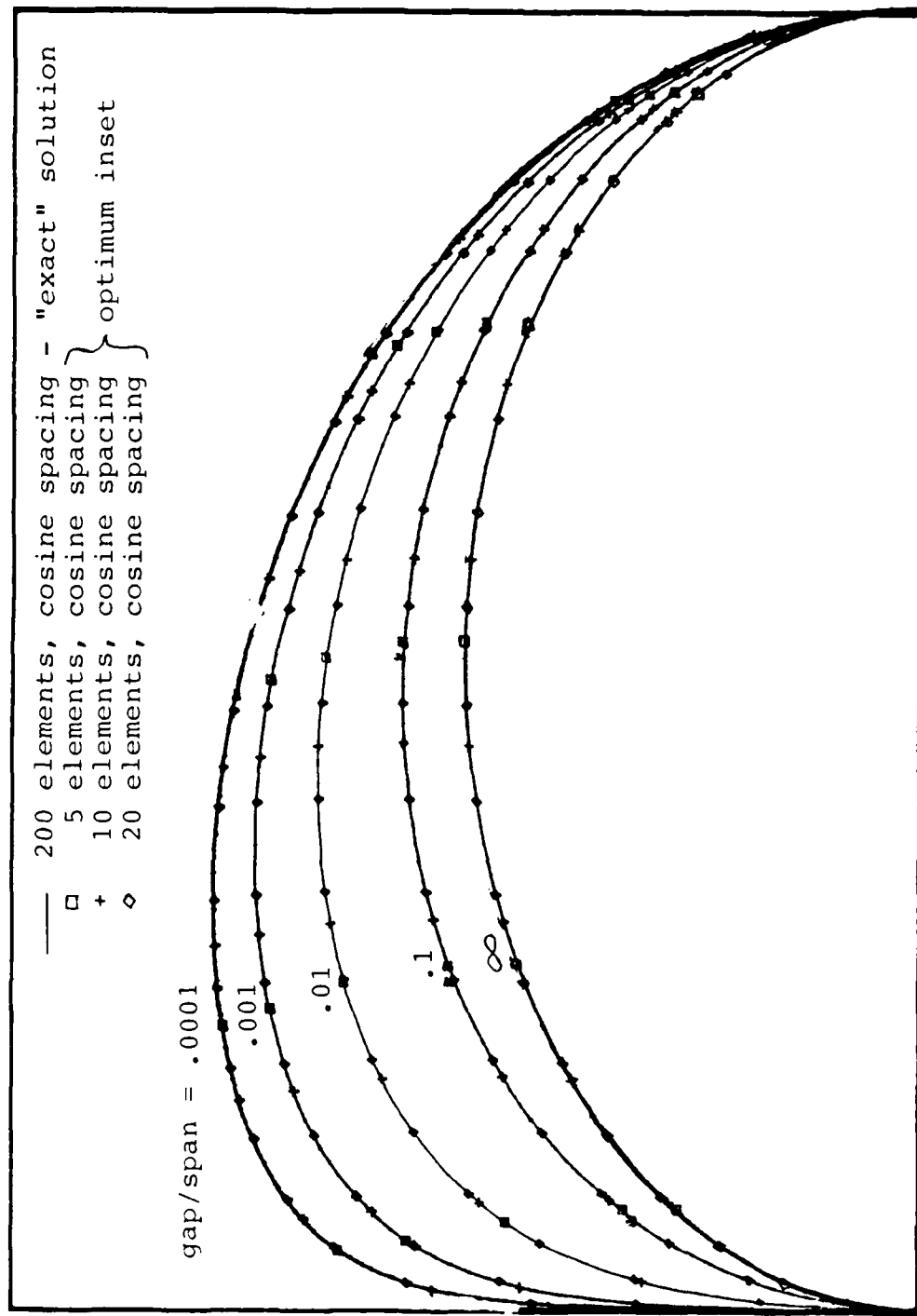


Figure 3.4 Circulation distribution on optimally loaded lifting line normal to wall, at various gap ratios. Comparison of "exact" solution with optimum 5, 10, and 20 element solutions, cosine spacing.

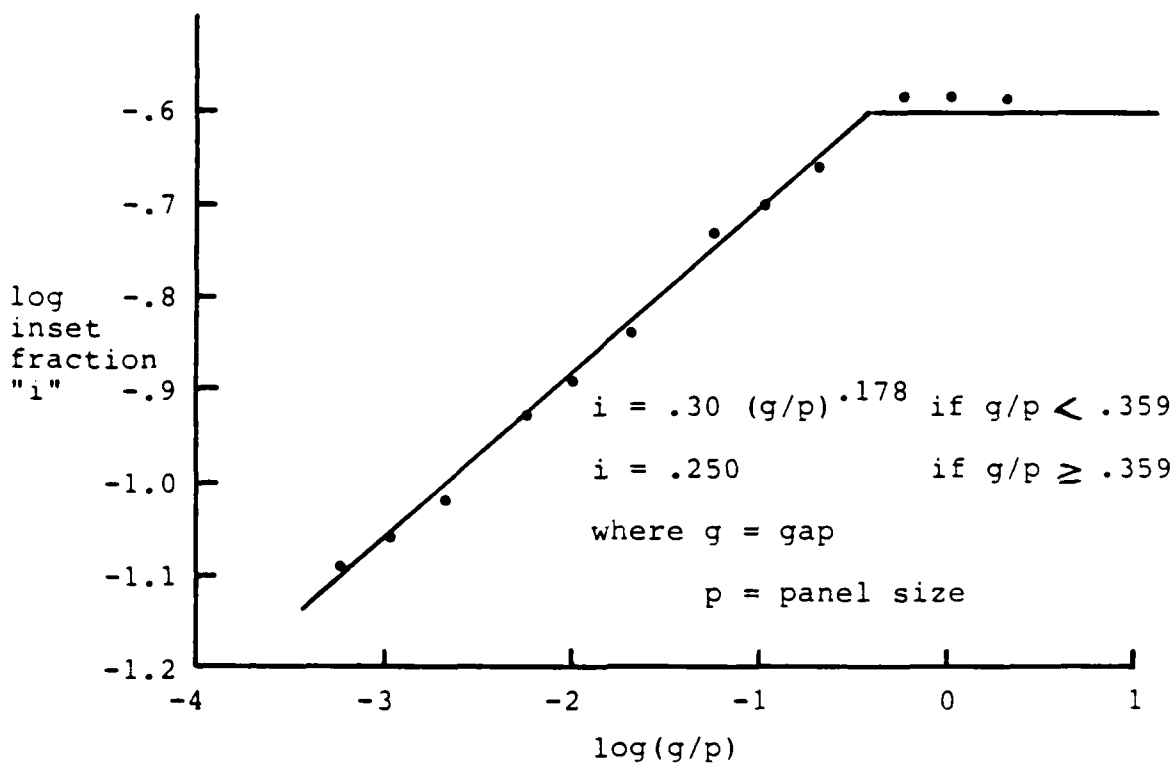


Figure 3.5 Optimum inset fraction, infinite wall, linear spacing.

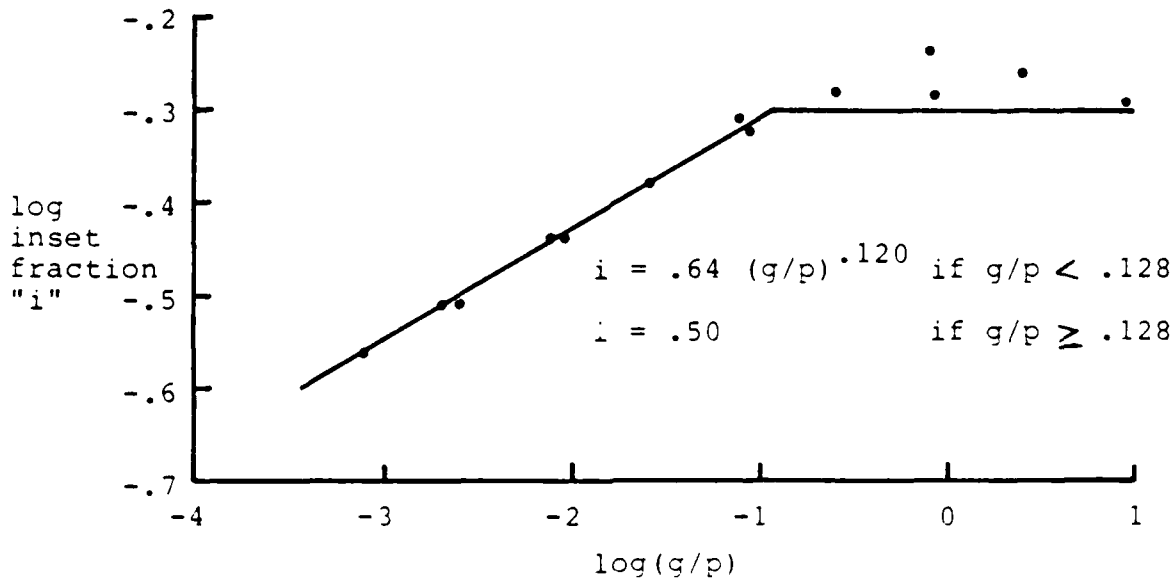


Figure 3.6 Optimum inset fraction, infinite wall, cosine spacing.

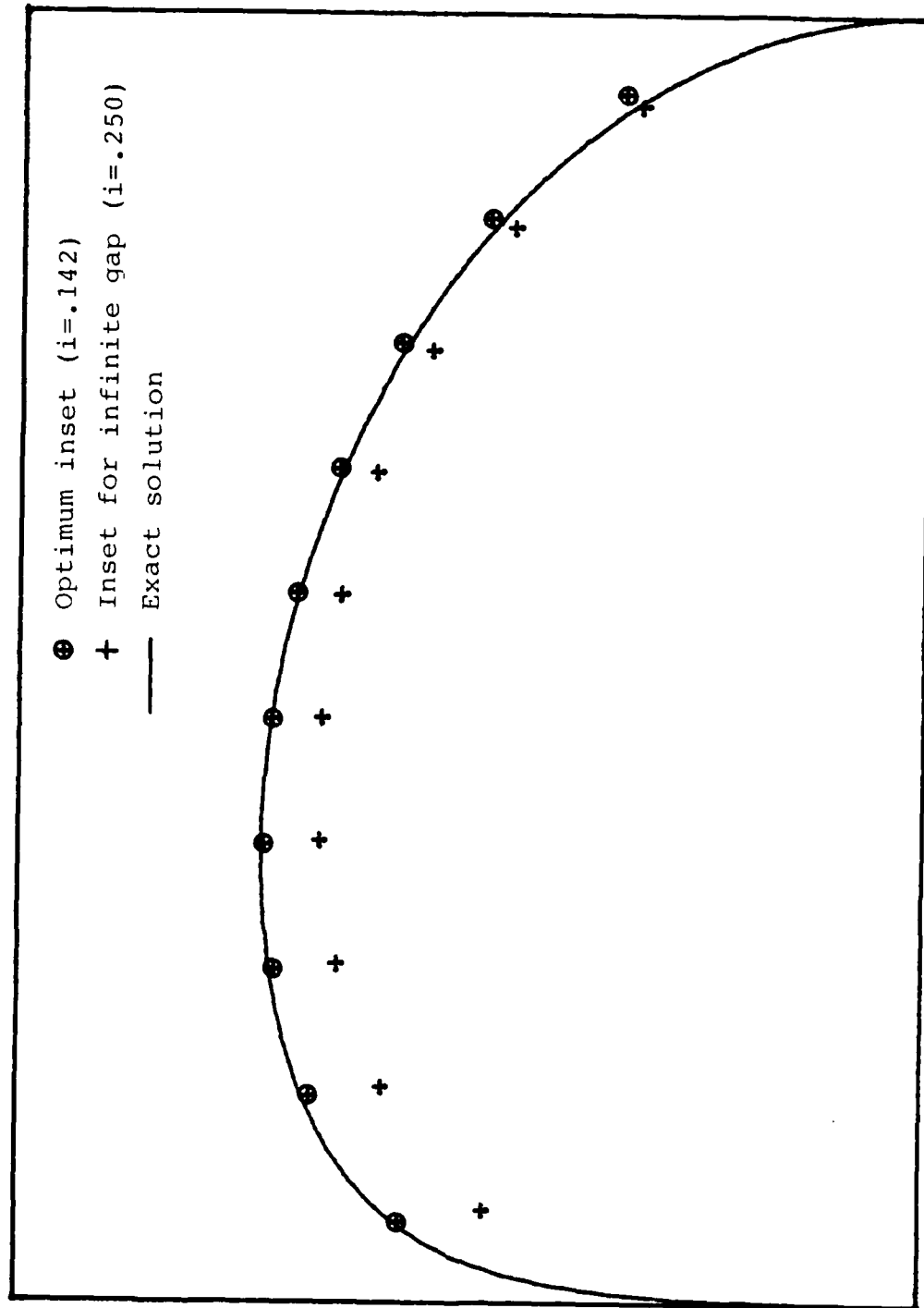


Figure 3.7 Circulation distribution on optimally loaded lifting line normal to wall. Gap/span = .001 10 discrete vortices, linear spacing. Comparison of optimum inset with infinite gap inset.

insets fall close to a single line, an approximate expression for which is given in the respective figures. In the large gap ratio region the expression deviates somewhat from the calculated optimum, but the solution is quite insensitive to inset at these gap ratios. At the lower gap ratios, the solution is much more sensitive, as can be seen in figure 3.7, where the optimum linear 10 vortex solution is shown for a gap of .001 span (optimum inset ratio = .142), as well as the 10 vortex solution using the isolated airfoil inset fraction of .25. In this case, the incorrect inset results in an error in induced drag of 10.2%.

The second numerical experiment concerned a wing separated by a small gap from a perpendicular, symmetrical, winglet of equal span. This winglet can be thought of as representing the duct surface in the case of a ducted propeller. The lifting line representation of this arrangement using linear spacing is shown in figure 3.8. The panelling of the main foil is the same as that used in the case of a foil near a wall. Each half of the winglet is panelled using the infinite gap inset at the free end and zero inset at the winglet's midspan position. The number of panels on the winglet was selected so that the distance from the center trailing vortex to the nearest control point matched as nearly as possible the distance between the last trailer and control point on the main foil. The "exact"

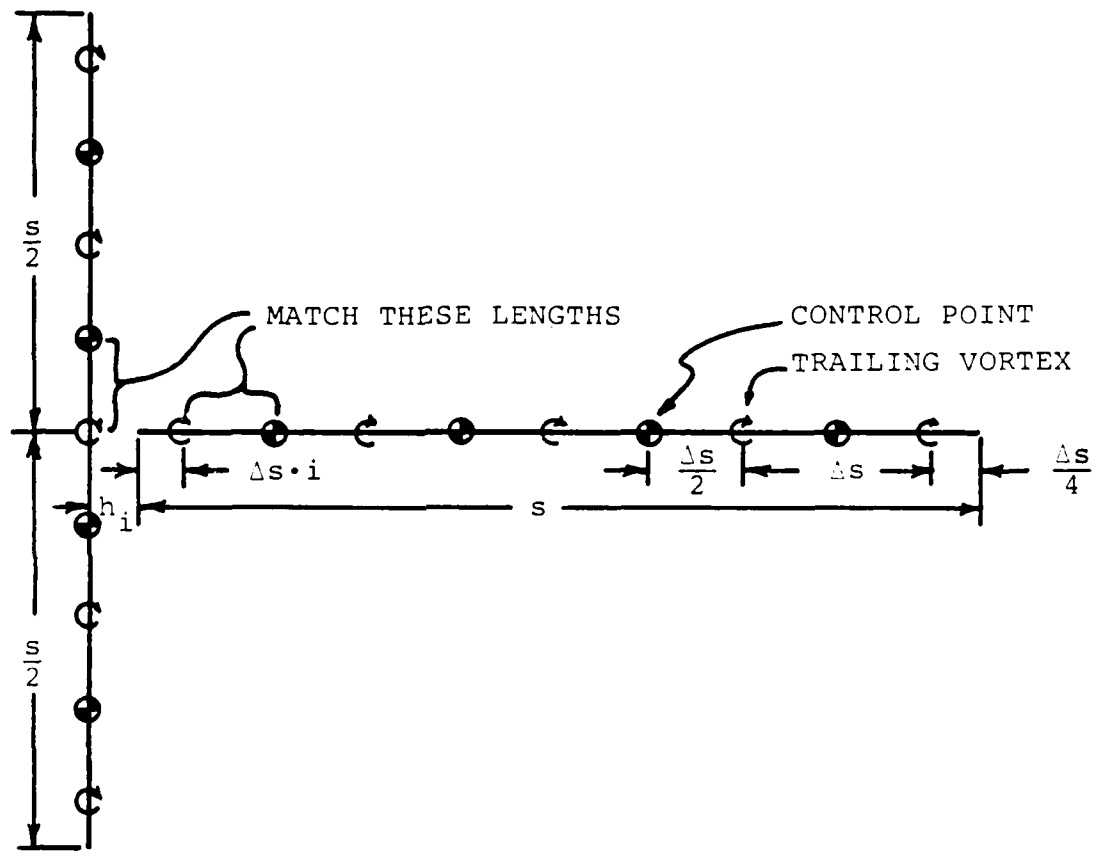
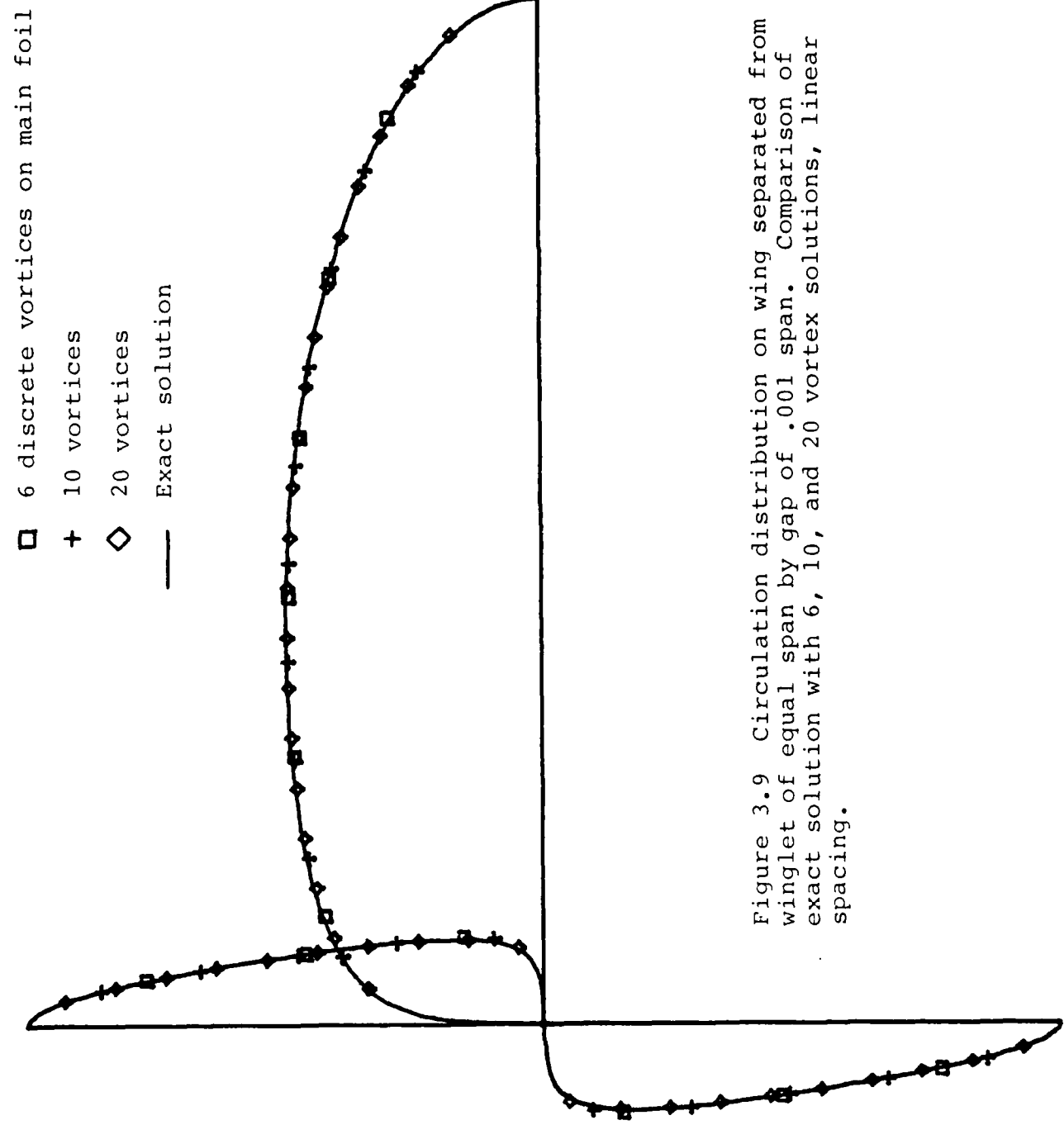


Figure 3.8 Winglet lifting line geometry, linear spacing.

minimum drag solution was found by using a large number of vortices and requiring the downwash on the foil to be a constant, and the sidewash on the winglet to be zero. The calculation was then repeated using fewer vortices, and varying the inset until the solution agreed most closely with the "exact" one. Figure 3.9 shows as an example the case of a gap of .001 span, and the optimum solution using 6, 10, and 20 vortices on each foil. The optimum inset fractions for linear and cosine spacing are given in figures 3.10 and 3.11. These values were used in the ducted propeller program.



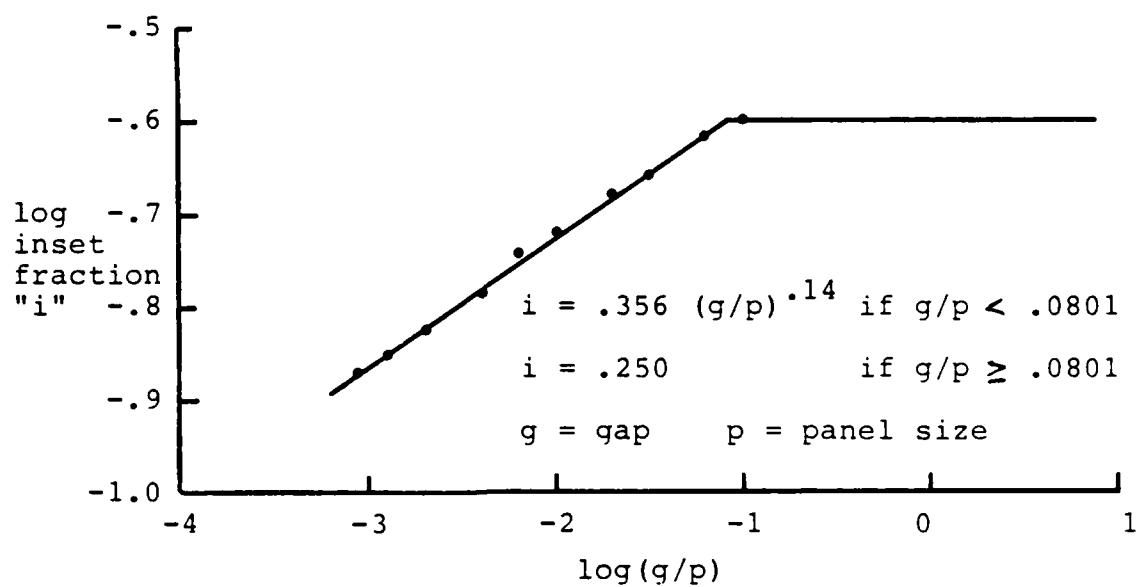


Figure 3.10 Optimum inset fraction for winglet with gap, linear spacing.

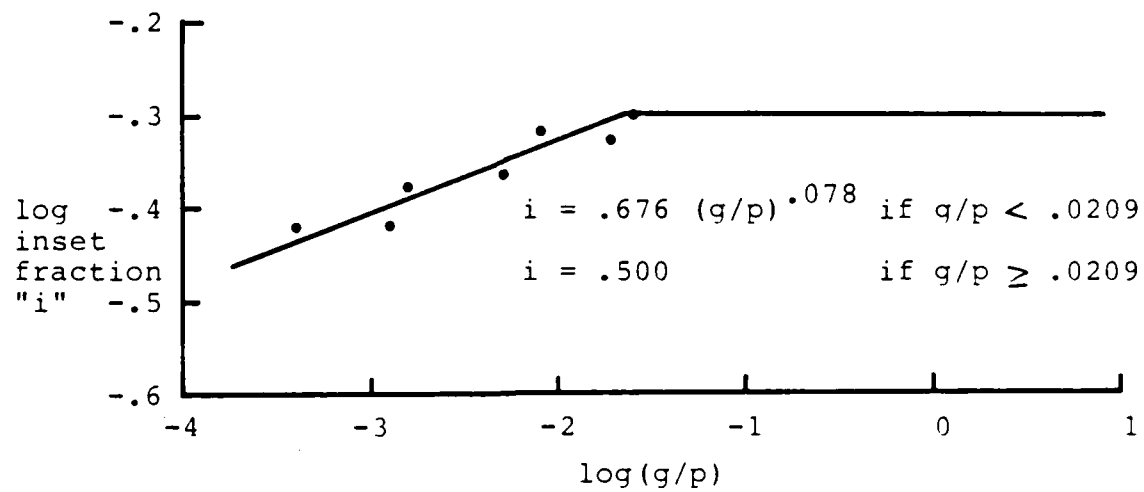


Figure 3.11 Optimum inset fraction for winglet with gap, cosine spacing.

4. VORTEX LATTICE REPRESENTATION OF FLOWS WITH TIP GAPS

In order to investigate the applicability of the optimum insets to non-optimally loaded foils, a planar lifting surface program was used to analyze a rectangular flat plate at an angle of attack, placed normal to an infinite wall from which it is separated by a gap. The insets used were those found optimum for a lifting line normal to an infinite wall. Cosine spacing (Lan, 1974) was used in the chordwise direction, and either cosine or linear spacing was used in the spanwise direction. The drag was calculated using Lan's method of deriving the suction force from the total upwash at the leading edge. The effective aspect ratio was then defined as

$$A_e = \frac{C_L^2}{\pi C_D}$$

Figures 4.1 and 4.2 show results for a geometric aspect ratio of 3 and a gap-to-span ratio of .001. The number of spanwise panels NS was varied from 3 to 24 while the ratio between the number of spanwise panels to the number of chordwise panels NC was kept constant, and equal to 3. It can be seen that the convergence was quite good for both linear and cosine spacing. Also shown are the corresponding results obtained using a vortex inset fixed at the infinite gap value. It can be seen that while the cosine spacing results converged quickly for this gap regardless of the

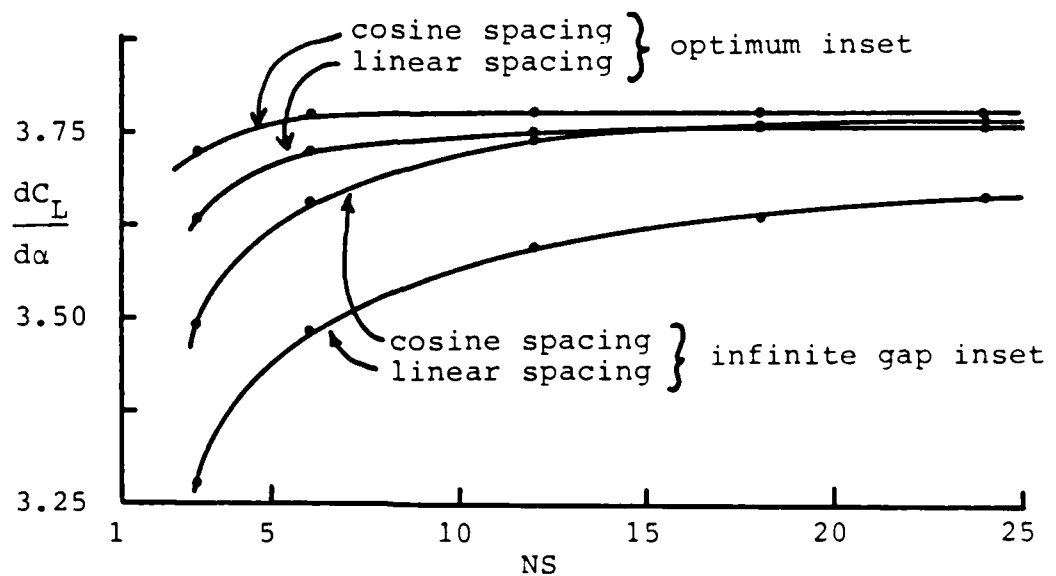


Figure 4.1 Convergence of lift curve slope, rectangular wing normal to infinite wall. Aspect ratio = 3. Gap/span = .001. NS/NC = 3.

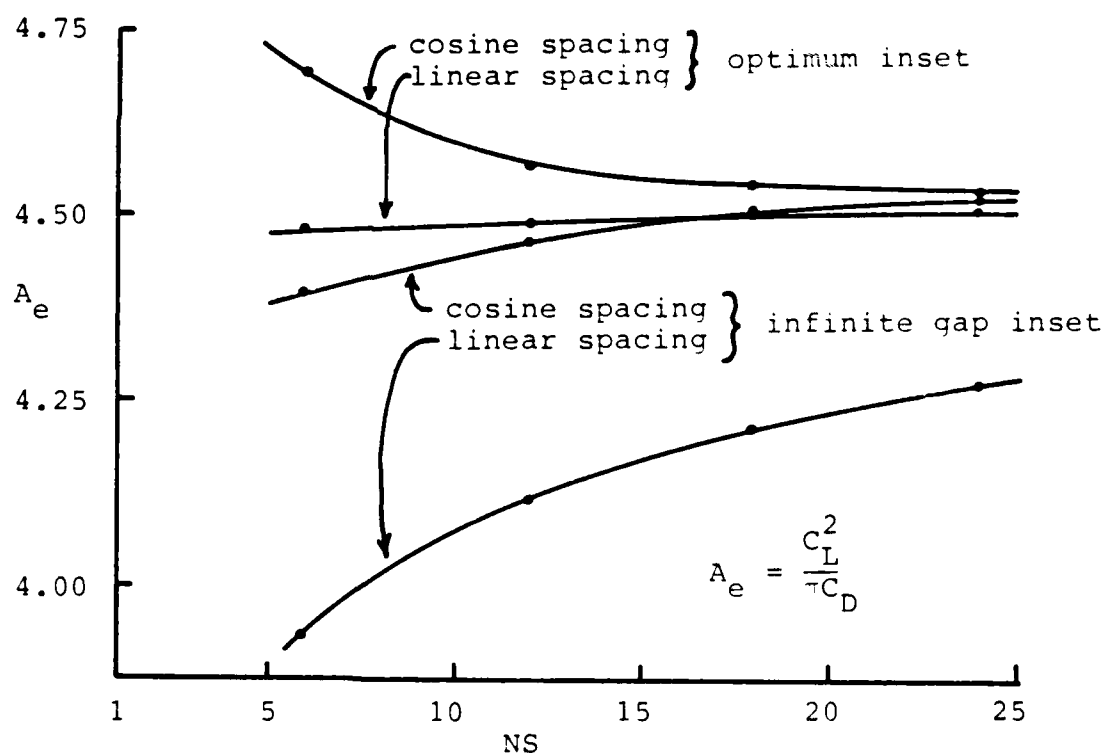


Figure 4.2 Convergence of effective aspect ratio, rectangular wing normal to infinite wall. Aspect ratio = 3. Gap/span = .001. NS/NC = 3.

inset, the convergence of the linear spacing results improved significantly when the optimum inset was used.

Figure 4.3 shows the calculated increase in the effective aspect ratio as the gap size is decreased, along with corresponding results for an optimally loaded foil from the lifting line calculation, and from a conformal mapping solution reported by Durand (1963). Surprisingly, this relationship appears to be practically identical for the two loading situations. Also shown are the experimental results of Munk and Cario (1917), as reported by Hoerner (1965), which indicate that the effect of the gap between two foils of aspect ratio 3 is significantly less than that predicted by lifting surface theory. This data is plotted assuming that $C_Q = 1$. Hoerner gives the Reynolds number, based on chord length, as 80,000, but gives no thickness data. The scaling arguments presented in Appendix A indicate that even for quite thick airfoils, the flow through the gap should be essentially inviscid for gap/span ratios as large as .01. The discrepancy between the calculated and measured effect of a small gap seems too large to be accounted for by deviations of C_Q from unity. Other experimental data presented by Hoerner and Borst (1975) and by Kerwin, Mandel, and Lewis (1972) deal with a control surface normal to a plane. These data also indicate that small gaps have a smaller effect than theory predicts.

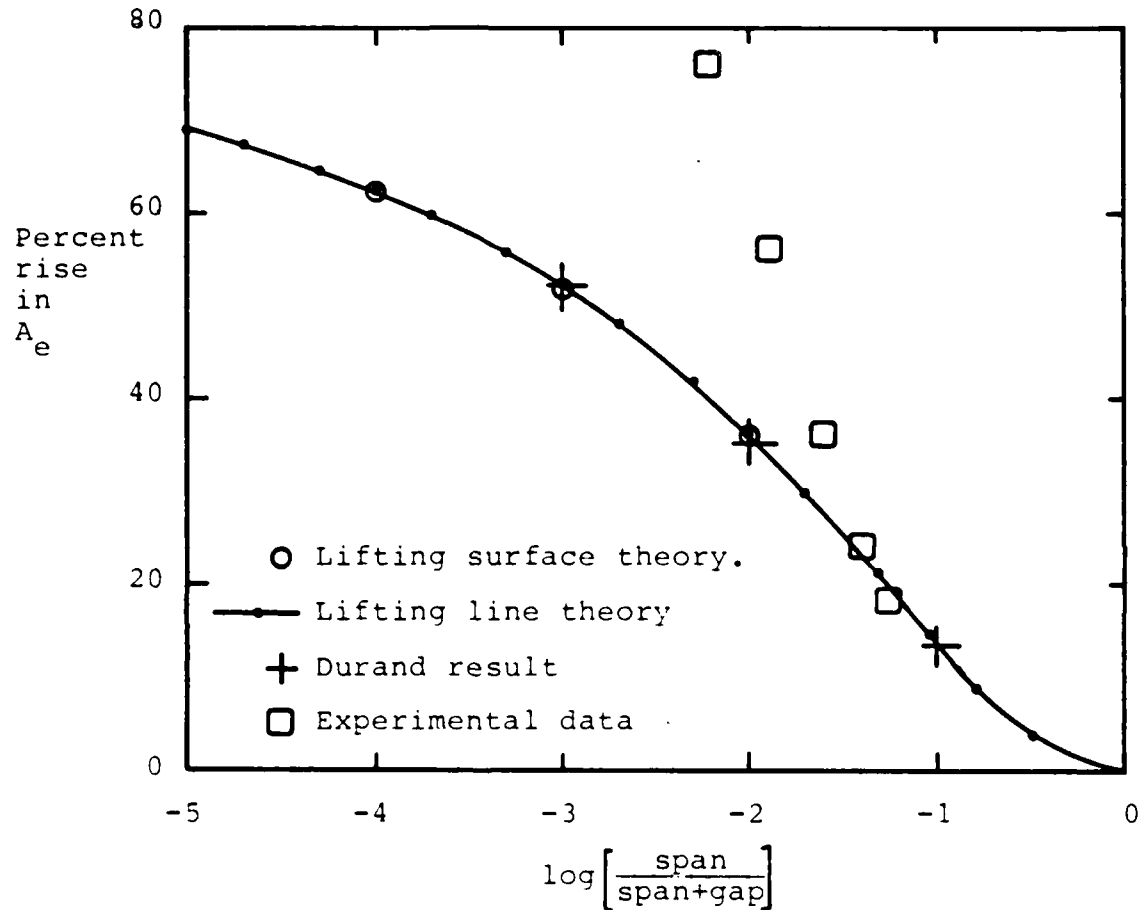


Figure 4.3 Percent rise in effective aspect ratio as foil approaches infinite wall. Comparison of lifting surface theory for rectangular foil of aspect ratio 3 with lifting line theory and results of Durand (1963) for optimally loaded foil. Experimental data from Hoerner (1965).

5. THE DUCTED PROPELLER ANALYSIS PROGRAM

The Ducted Propeller in Steady Flow (DPSF) program is an adaptation of PSF, developed by Greeley (1982) and described by Greeley and Kerwin (1982). DPSF analyses ducted and banded propellers operating in an axisymmetric inflow consisting of axial, radial, and tangential components. This inflow field is generally taken to be the circumferential average velocity field at the propeller plane, and can include the effects of stators and multiple rotors. The presence of the propeller hub and any other boundaries to the flow is not modeled. The blade and duct boundary layers are assumed to be thin, so that the flow can be considered inviscid, except for the empirical addition of frictional drag.

The blades and duct are represented by straight-line vortex and source lattice elements of constant strength that are distributed over the mean camber surface. The trailing vorticity in the wake of the propeller is represented by straight-line vortex elements distributed over a specified surface. The vortices are arranged in horseshoe vortices so as to satisfy Kelvin's condition, and the strength of the horseshoe vortices is determined by solving a set of simultaneous equations, each satisfying the flow tangency condition at a control point. Source strength is determined stripwise using a linearized boundary condition.

The position of the trailing vortex wake is determined iteratively by first solving the boundary value problem with a guessed position, and then aligning the wake with the computed velocity field. The boundary value problem is then re-solved and the procedure is repeated until convergence is obtained. When a converged solution is obtained, blade forces are found by application of the Kutta-Joukowski and Lagally theorems.

Blade Geometry

The description of blade geometry in DPSF is as shown in figure 5.1. The coordinates of the midchord line are defined by the radial distribution of skew angle $\theta_m(r)$ and rake $x_m(r)$. The pitch angle $\phi(r)$ and chord $c(r)$ define the angle and extent of the sectional nose-tail line along the surface of a cylinder of constant radius r . The camber $f(r,s)$ and thickness $t(r,s)$ describe the section characteristics of the blade as a function of radius, r , and the fraction of chord from the leading edge, s . The camber is measured along the cylindrical surface at right angles to the nose-tail line. The thickness is measured normal to the mean line. The propeller radius, R , is defined as the maximum radius of the blade midchord line.

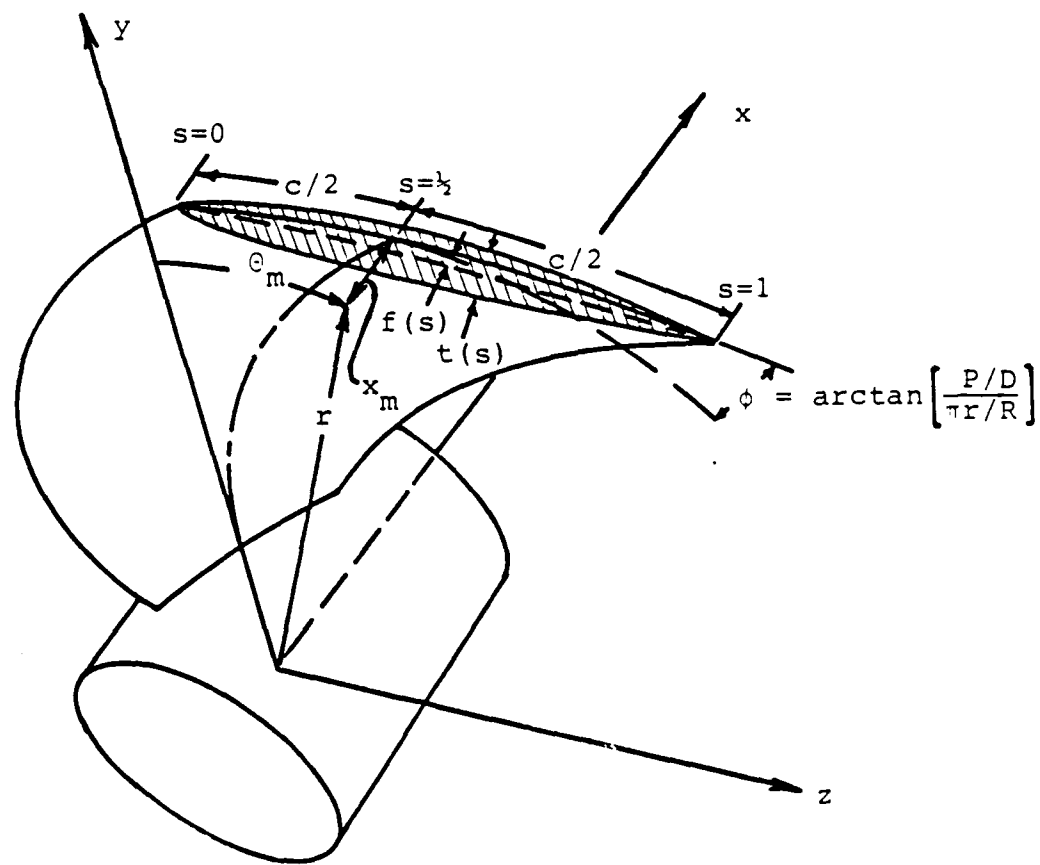


Figure 5.1 Blade geometry.

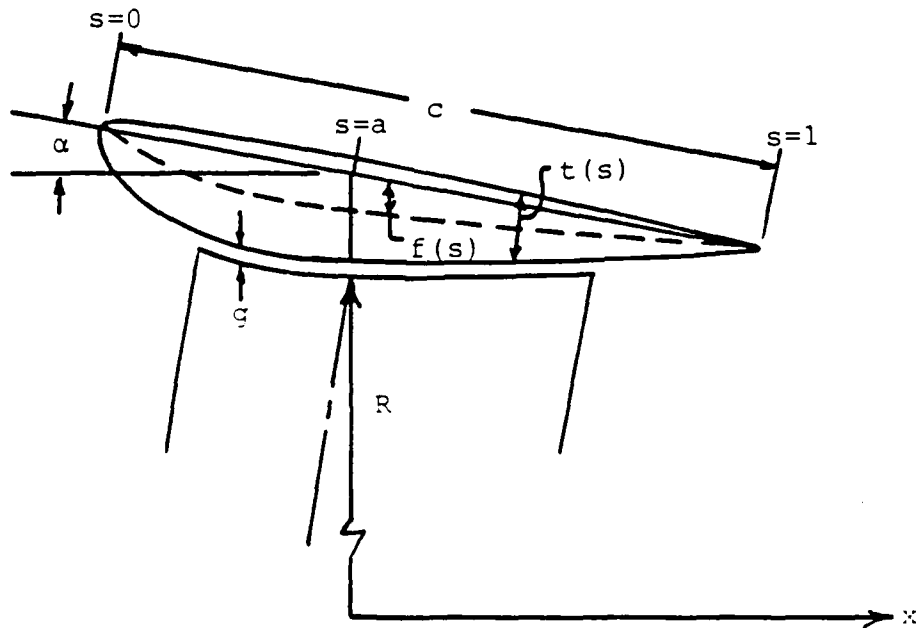


Figure 5.2 Duct geometry.

All geometric properties describing the blade must be defined out to a radius equal to the largest radial extent of the blade surface, which is likely to exceed that of the midchord line. This avoids the uncertainty involved in extrapolation.

Duct Geometry

The duct (or band) is assumed to be axisymmetric and is defined in terms of its chord c , chord fraction forward of the blade tip midchord line "a", angle of attack α , camber $f(s)$, and thickness $t(s)$. The gap g between the blade tip and the inner surface of the duct is assumed to be constant, and may be zero, as in the case of a banded propeller. Unlike BPSF (Van Houten, 1983), all quantities are defined in the (r,x) plane, as shown in figure 5.2. Note that duct camber is applied in the radial direction only.

Vortex Lattice

The vortex lattice representing the propeller geometry consists of spanwise and chordwise vortices. The lattice representing the blade is located on the blade camber surface. That representing the duct follows the duct camber surface, but is displaced radially inward so that its

distance from the blade tip is equal to the physical tip gap. A typical vortex lattice is shown in figure 5.3.

The spanwise spacing of the chordwise vortices on the blade and duct can be independently selected to be either linear, cosine, or in the case of the duct, a mixture of the two. With linear spacing the intersection of the blade chordwise vortices with the midchord line is given by:

$$r_m = \frac{(R - r_H)(m - .75)}{M + .25 + i} + r_H \quad m = 1, 2, \dots, M+1$$

where r_H is the hub radius and M is the number of spanwise panels. The inset fraction i is given in figure 3.10, where the panel size is equal to $r_{M+1} - r_M$.

In the case of cosine spacing, the corresponding relationship is:

$$r_m = .5(1 - \cos(\hat{r}_m))(R - r_H) + r_H \quad m = 1, 2, \dots, M+1$$
$$\hat{r}_m = \frac{(m - .5) \pi}{(M + .5 + i)}$$

where the inset fraction is given in figure 3.11.

The radial position of each chordwise vortex varies as it crosses the blade. The outermost chordwise vortex follows the duct camber line. The other chordwise vortices have a radial variation which is attenuated by the factor

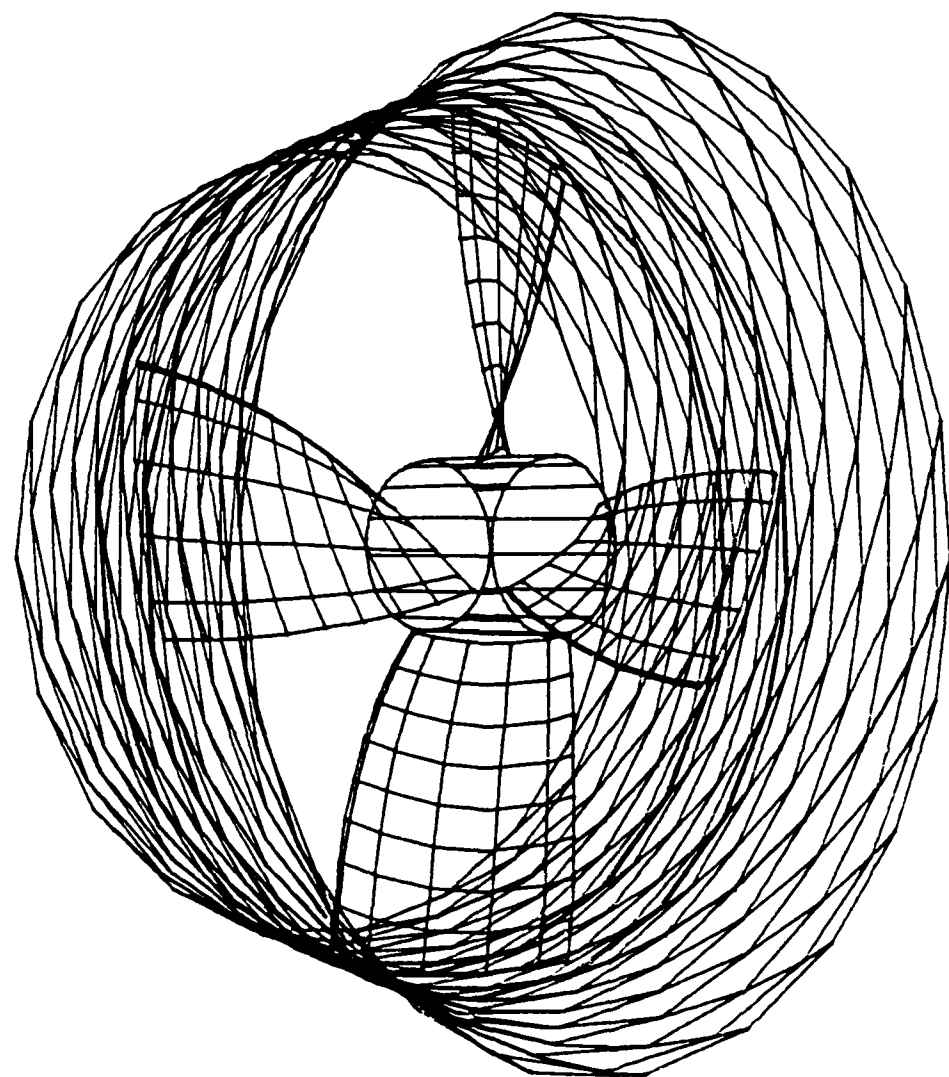


Figure 5.3 Vortex lattice for NSMB Ka4-55 propeller in Nozzle 19.

$$(r_m - r_H) / (R - r_H).$$

The spanwise position of control points depends on the type of spacing used. With linear spacing, the control points are located midway between chordwise vortices. With cosine spacing the i th control point is located at a position corresponding to a value of \hat{r} midway between \hat{r}_i and \hat{r}_{i+1} .

One of the duct's chordwise vortices is always located along the blade tip, displaced radially outward by the gap. The extension of this vortex beyond the blade leading edge follows the slope of the blade camber surface at the leading edge. The extension beyond the blade trailing edge follows the current wake geometry. The other chordwise vortices on the duct are displaced circumferentially from this vortex by an amount θ_m which depends on the spacing used. With linear spacing,

$$\theta_m = \frac{(m-1) 2 \pi}{M_d z} \quad m = 1, 2, \dots, M_d + 1$$

where M_d is the number of spanwise panels on each duct segment, and z is the number of blades. With cosine spacing,

$$\theta_m = \pi(1 - \cos \hat{\theta}_m) / Z$$

$$m = 1, 2, \dots, M_d + 1$$

$$\hat{\theta}_m = (m-1) \pi / M_d$$

With mixed spacing:

$$\theta_m = 2 \pi / Z [b \left(\frac{m-1}{M_d} \right) + .5(1-b) (1 - \cos(\hat{\theta}_m))]$$

where b can vary between 0 (cosine spacing) and 1 (linear spacing). The spanwise position of control points follows that used on the blades.

The spacing method used and the number of panels used on the blade and duct must be chosen carefully. It is recommended that the distance between the last blade control point and the last blade chordwise vortex match as closely as possible the distance between the duct chordwise vortex at the blade tip and the nearest duct control point.

The spanwise vortices on the blade are located at constant values of s , the variable which varies from 0 to 1 along the chord. The chordwise spacing of these vortices can be selected to be linear:

$$s_n = (n - .75) / N \quad n = 1, 2, \dots, N$$

or cosine:

$$s_n = .5 (1 - \cos (\hat{s}_n))$$
$$\hat{s}_n = \pi (n - .5) / N$$
$$n = 1, 2, \dots, N$$

where N is the number of panels chordwise. With linear spacing the i th control point is located midway between the i th and $(i+1)$ th spanwise vortex. In the case of cosine spacing the i th control point is located at the value of s corresponding to a value of \hat{s} midway between \hat{s}_i and \hat{s}_{i+1} .

Spanwise vortices are located on the duct at the same axial locations as the end points of the spanwise vortices on the blade. In addition, the portions of the duct extending beyond the blade leading and trailing edges are represented by spanwise vortices spaced using the same scheme (linear or cosine) as the blade and central portion of the duct. A minor exception to this is that when using cosine spacing the trailing portion of the duct is panelled "half-cosine", where:

$$\hat{s}_n = \frac{\pi (n - .5)}{(2N + .5)}$$

$$s_n = (1 - \cos (\hat{s}_n))$$

The spacing scheme and the panel numbers used should be selected so that the panel size varies smoothly between the mid-portion of the duct and the portion extending beyond the

blade leading and trailing edges. In the case of linear spacing, the number of panels on the different portions of the duct should be proportional to their respective axial extent. In the case of cosine spacing, there are control points on the duct at the axial position of the blade tip leading and trailing edges. These control points should be as nearly as possible midway between the adjacent spanwise vortices.

In DPSF, all blades (and all segments of the duct) are panelled identically. This causes run times to be somewhat longer than if the "non-key" blades were panelled more coarsely, but the code is significantly simplified.

Wake Geometry

The geometry of the blade transition and ultimate wakes in DPSF is similar to that in PSF, as described by Greeley and Kerwin (1982). One difference is that the transition wake is "grown" by increments in x , rather than θ . Those wake points forward of the duct trailing edge are located at values of x corresponding to the spanwise vortices on the duct. Behind the duct trailing edge, the wake is grown by an axial increment which is specified by the user. The radial location of the blade trailing vortices aft of the duct trailing edge follows PSF. Forward of the duct

trailing edge the radius of the m th trailer is contracted by an amount equal to $(r_m - r_H) / (R - r_H)$ times the contraction of the duct camber line between the blade trailing edge and the axial position of the wake point in question. The duct transition wake is modeled by a set of trailing vortices which begin where the duct chordwise vortices intersect the trailing edge of the duct, and parallel the outermost trailing vortex from the key blade, displaced by the same angle as that of the chordwise vortex on the duct. The ultimate wake is modeled the same as in PSF.

Wake Alignment

The blade transition wake is aligned the same way as in PSF, except for the case of the outermost blade trailing vortex. In PSF, the velocity calculated on this vortex includes a self-induced velocity due to the curvature of the rolled-up tip vortex. Since in the case of a ducted propeller the roll-up of the tip vortex is impeded by the presence of the duct, DPSF does not include this term. The velocity induced at a segment of the outermost blade trailing vortex due to itself and the adjacent segments of duct chordwise and spanwise vortices is calculated by assuming that the vorticity in these segments is spread out over the local duct panel. The magnitude of the local

velocity is just one half the resulting vortex density.

Because the duct chordwise vortices aft of the blade trailing edge are aligned with the blade transition wake, this portion of the duct must be repanned after each iteration of wake alignment.

Source Strength

As in PSF, the blade thickness is represented by line sources at the same location as the spanwise vortices. Their strength is obtained by using thin wing theory, based on the undisturbed inflow velocity. This undisturbed inflow velocity is calculated at the mean radius of the source element at the midchord position. The strength of the line sources on the duct are calculated in the same way as those on the blade.

Solution of Boundary Value Problem

The solution of the boundary value problem in DPSF follows the procedure in PSF exactly. The number of additional unknowns representing bound vorticity on the duct is exactly equal to the number of additional equations to be solved in order to enforce flow tangency on the duct control

points.

Force Calculation

The calculation of forces in DPSF is practically the same as that in PSF. The total velocity is calculated at the midpoint of each singularity, and the Kutta-Joukowski and Lagally theorems applied. The only exception to this is that the Lagally forces on the sources due to the undisturbed relative inflow is not included. This is necessary in order that the Coriolis force on the fluid emitted by the sources does not contribute to shaft torque (Van Houten, 1983).

The forces on the individual singularities are summed up to give overall forces and moments on each spanwise panel. The force associated with each spanwise panel on the blade and duct includes the forces on the spanwise singularities in that panel and one half the forces on the chordwise vortices on the edge of the panel. The forces on the innermost and outermost panels include the entire forces on the innermost and outermost chordwise vortex, respectively. These panel forces are then summed to give the forces on the blade, the duct, and the complete propeller. The torque exerted on the duct can be included in the propeller torque or not, depending on whether it in fact represents a duct or

a band.

The empirical viscous drag force added to the force on each spanwise vortex is computed from the local velocity, the area of the local panel, and an estimated drag coefficient. In order to account for an increase in the drag at non-ideal angles of attack, the chordwise force calculated on the spanwise vortices nearest the leading edge is multiplied by a suction force coefficient that lies between zero and unity (Kerwin and Lee, 1978). The drag and suction force coefficients are allowed to vary radially along the blade and can be prescribed separately on the duct. For thin sections typical of propeller blade tips, a suction force coefficient of 0.333 is generally used (Kerwin and Lee, 1978; Greeley and Kerwin, 1982). For thicker sections, such as those used on typical ducts, larger values are probably appropriate.

Results

In order to assess the accuracy of DPSF performance predictions, comparisons were made with published experimental open water curves for both a banded propeller and a ducted propeller.

The banded propeller investigated was one of NSMB's R4-55 series, data for which were given by Van Gunsteren (1970). These are 4-bladed propellers with an expanded area ratio of .55. They have zero skew and rake, and nominal P/D ratios of 1.0, 1.2, 1.4, 1.6, and 1.8. The blades have NACA $a=.8$ mean lines, and 16-series thickness sections. The 1.4 P/D propeller was chosen for the comparison between experimental results and the predictions of DPSF. The geometry for this propeller is tabulated in Table 5.1. Although the nominal diameter of this propeller is 240 mm, the actual radius, as defined in DPSF was 237.2, so calculated values of K_T , K_Q , and J were adjusted accordingly.

DPSF calculations were made using 8 spanwise panels and 9 chordwise panels on the blade. The band had two chordwise panels forward of the blade leading edge and one panel aft of the blade trailing edge. The band had 7 spanwise panels between blade tips. Cosine spacing was used chordwise and linear spacing used spanwise. The vortex lattice is shown in figure 5.4. Calculations were made at advance ratios of 0, .247, .494, .741, .988 and 1.235. The wake was not contracted radially. The viscous drag coefficient was taken to be .0085. The suction force coefficient was assumed to be .333 on the blade and 1.0 on the band.

NSMB PROPELLER R4-55

r/R	c/D	t/D	f/c	P/D	θ_m	x_m
.182	.179	.039	.0175	1.423	0.0	0.0
.300	.208	.031	.0199	1.402	0.0	0.0
.400	.232	.023	.0215	1.389	0.0	0.0
.500	.254	.016	.0226	1.380	0.0	0.0
.600	.273	.015	.0230	1.379	0.0	0.0
.700	.288	.015	.0225	1.386	0.0	0.0
.800	.299	.015	.0198	1.408	0.0	0.0
.900	.306	.015	.0135	1.446	0.0	0.0
.950	.308	.015	.0092	1.472	0.0	0.0
1.000	.309	.015	.0048	1.502	0.0	0.0

4 BLADES

a=.8 mean line

NACA 16 thickness distribution

BAND GEOMETRY

NACA 250 mean line, with 0024 thickness distribution
 $c/D = .1474$ $f/c = .0853$ $t/D = .0354$ $\alpha = 13.17^\circ$

Table 5.1 Geometry of NSMB R4-55 Banded Propeller

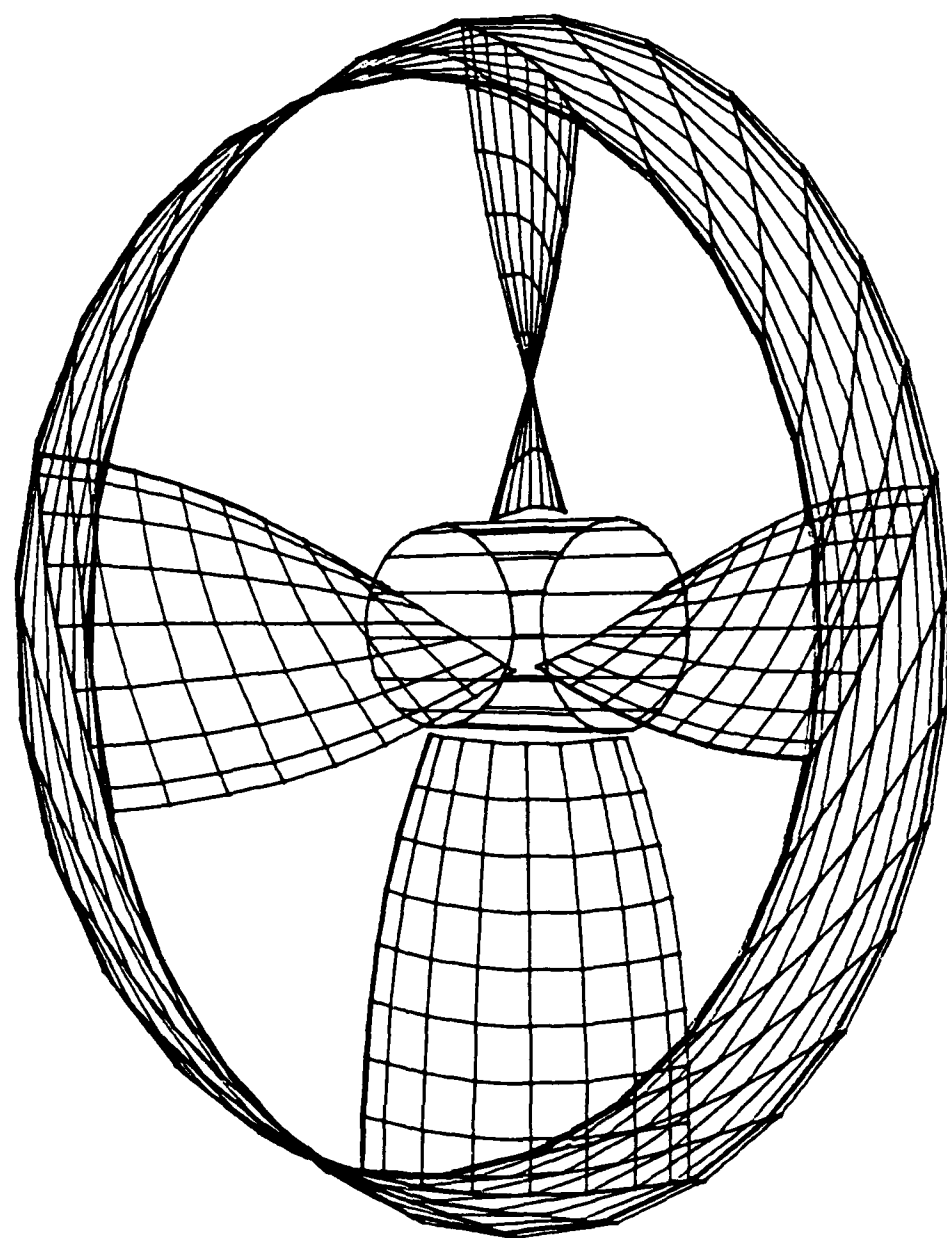


Figure 5.4 Vortex lattice for NSMB R4-55
banded propeller.

Calculated and experimental open water results are given in figure 5.5. The agreement is quite good, and is significantly better than that obtained using BPSF (Van Houten, 1983). The spanwise distribution of bound circulation is shown in figure 5.6. The transfer of vorticity from the blade tip to the band can be seen to be fairly complete.

The ducted propeller investigated was NSMB's Ka4-55 ducted propeller with a P/D of 1.0, operating in Nozzle 19, data for which is given by van Manen (1962). The blade geometry for this propeller is not described in terms of modern airfoil sections so for the purpose of running DPSF the geometry was approximated in terms of "equivalent" sections, as given in Table 5.2. The duct geometry was given in terms of a NACA section, so no approximation was necessary. The tip gap was 1 mm, or .42% of the 240 mm propeller diameter.

Calculations were made using 8 spanwise panels and 6 chordwise panels on the blade. The duct had 9 chordwise panels forward of the blade and 6 aft, for a total of 21 chordwise panels. 5 spanwise panels were used on each duct segment. Cosine spacing was used chordwise, and linear spacing was used spanwise. The complete vortex lattice is shown in figure 5.3. Calculations were made at advance ratios of 0, .18, .36, .54, .72, and .90. The wake

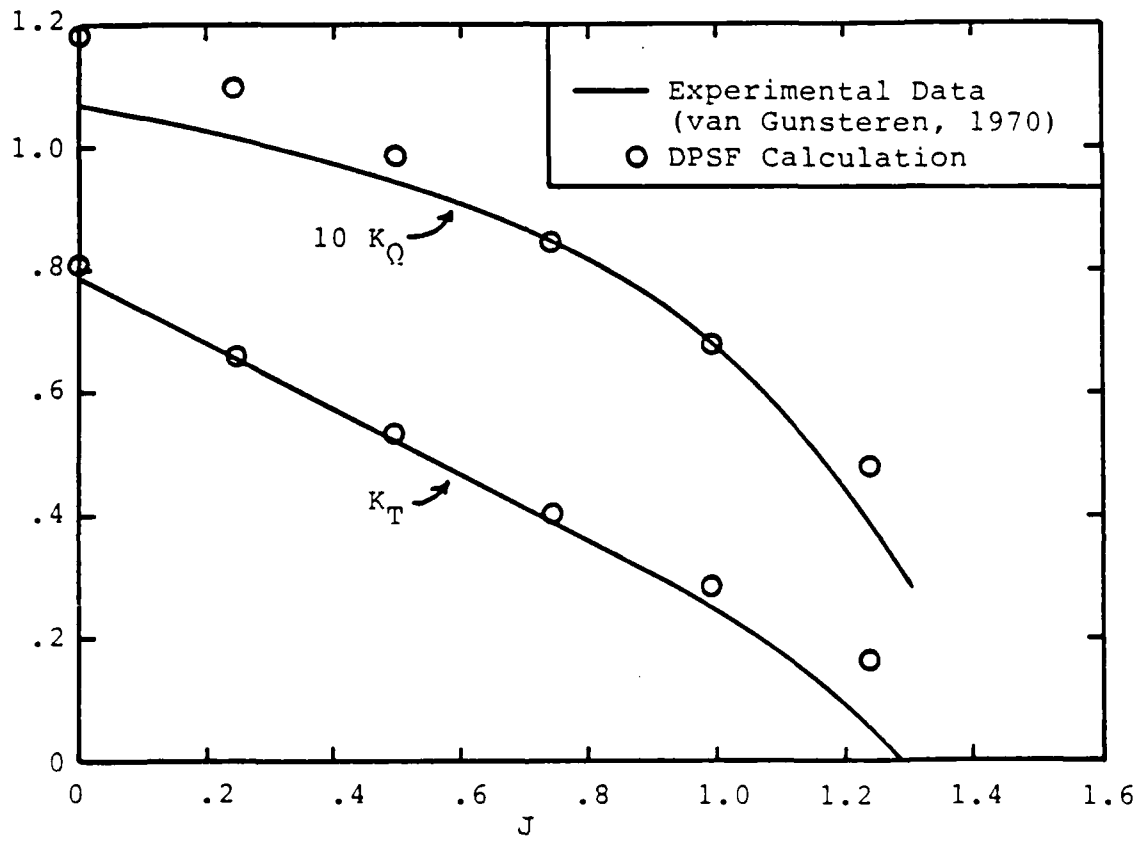


Figure 5.5 Comparison of calculated forces with experimental data for R4-55 propeller, $P/D = 1.4$.
 $(SFC = .333$ on blade, 1.00 on band; $C_D = .0085$)

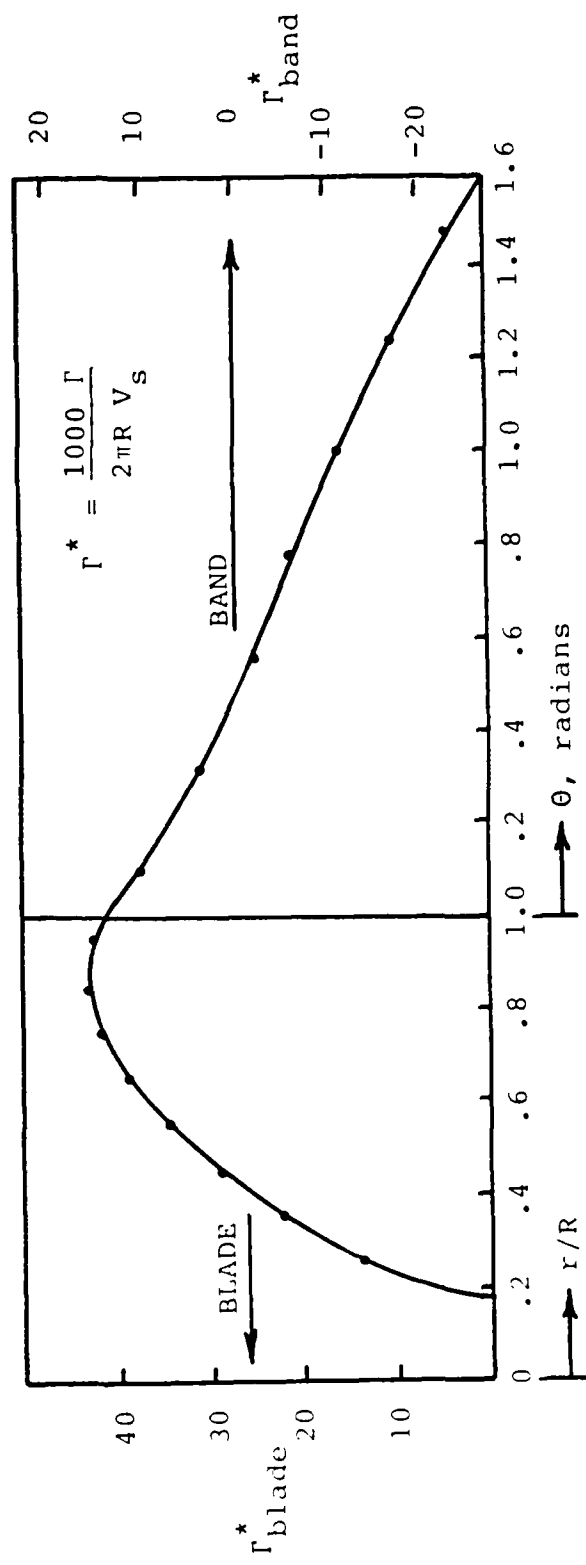


Figure 5.6 Spanwise distribution of circulation on blade and band,
R4-55 propeller at $J = .989$.

NSMB PROPELLER Ka4-55

r/R	c/D	t/D	f/c	P/D	θ_m	x_m
.200	.182	.0400	.0510	1.067	0.00	.0000
.300	.207	.0352	.0553	1.025	2.54	.0070
.400	.231	.0300	.0502	1.012	4.16	.0115
.500	.252	.0245	.0416	1.003	5.01	.0139
.600	.271	.0190	.0351	1.000	5.43	.0151
.700	.287	.0138	.0240	1.000	5.55	.0154
.800	.298	.0092	.0154	1.000	5.55	.0154
.900	.305	.0061	.0100	1.000	5.55	.0154
1.000	.306	.0050	.0082	1.000	5.55	.0154

4 BLADES

Parabolic mean line assumed

NACA 4-digit thickness distribution assumed

NOZZLE 19

NACA 250 mean line, with 0015 thickness distribution
 $c/D=.5$ $f/c=.07$ $t/D=.075$ $\alpha = 10.2^\circ$ $g/D=.0042$

Table 5.2 Approximate Geometry of NSMB Ka4-55 Propeller
 in Nozzle 19

contraction, viscous drag coefficient, and suction force coefficients were the same as for the R4-55 propeller.

Calculated and experimental open water curves are shown in figure 5.7. The total thrust was predicted quite accurately, but duct thrust and shaft torque were significantly in error. One run was made at $J=.36$ for a gap ratio corresponding to a 3 mm gap. The efficiency reduction of 1.9% fell on the curve given by van Manen for $Kt/J^2=3$.

The convergence of DPSF was tested by running the $J=.36$ case with 1.5 and 2 times the original number of chordwise panels and again with 1.5 and 2 times the original number of spanwise panels. The results are shown in Table 5.3. Blade forces did not vary by more than one percent. Duct thrust, however, increased by 28 percent as the number of chordwise panels was doubled. The reason for this slow convergence is not presently known.

Figure 5.8 shows the spanwise distribution of circulation on the blade and duct for the $J=.36$ condition. It can be seen that loading is transferred to the duct, but this effect is much less pronounced than in the case of a banded propeller.

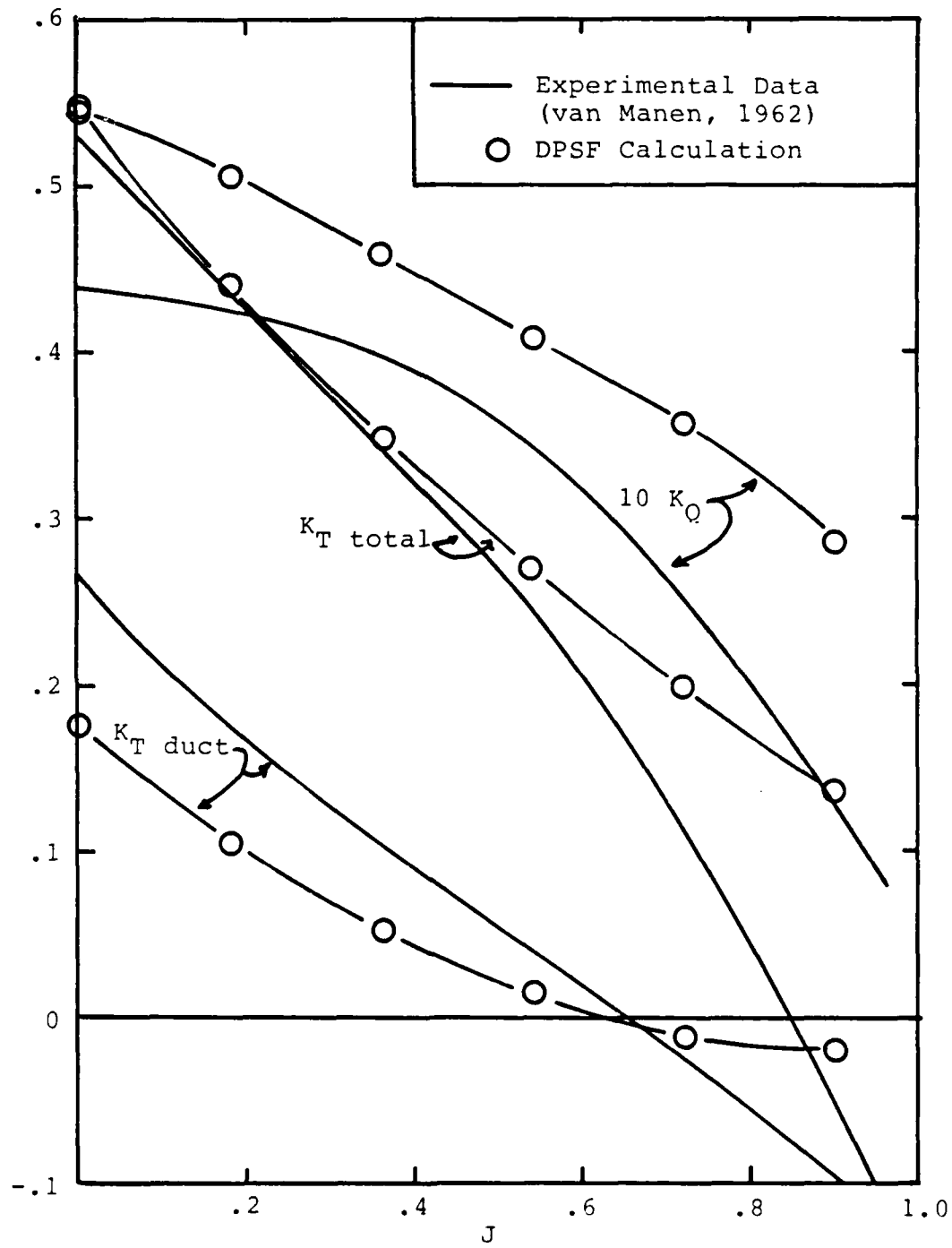


Figure 5.7 Comparison of calculated forces with experimental data for Ka4-55 ducted propeller, $P/D=1.0$.
 $(SFC = .333$ on blade, 1.00 on duct; $C_D = .0085$)

PANELLING	BLADE	DUCT	TOTAL	K_Q
	K_T	K_T	K_T	
Initial arrangement	.3017	.0481	.3498	.04651
x1.5 spanwise	.2993	.0415	.3408	.04641
x2.0	.2985	.0429	.3414	.04646
x1.5 chordwise	.3013	.0570	.3583	.04679
x2.0	.2993	.0617	.3610	.04670
----- DUCT -----				
INITIAL ARRANGEMENT:	BLADE	FWD	MID	AFT
Chordwise Panels	6	9	6	6
Spanwise Panels	8	5	5	5

Table 5.3 Results of convergence test on Ka4-55 propeller
at $J=.36$

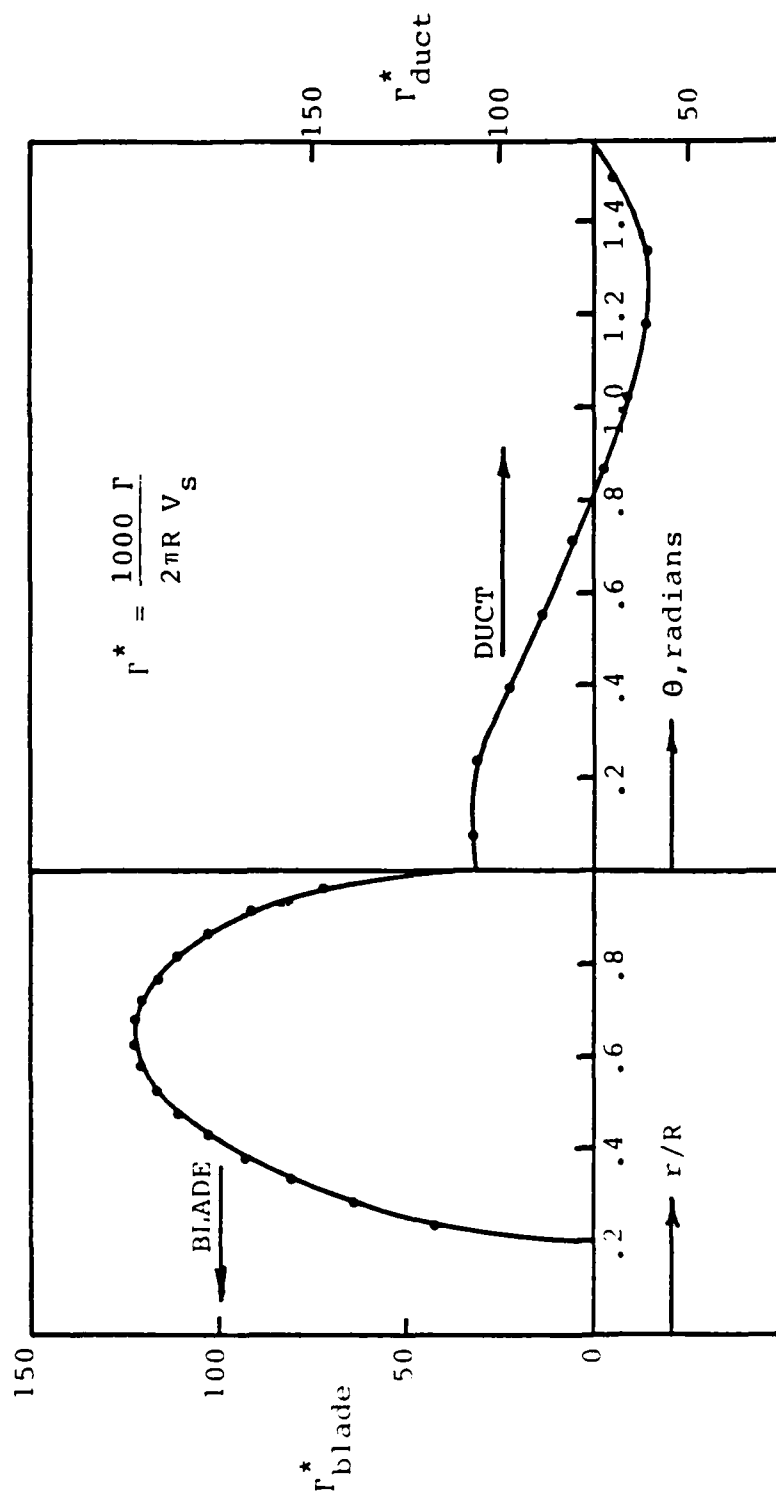


Figure 5.8 Spanwise distribution of circulation on blade and duct,
Ka4-55 propeller at $J = .36$.

Computation Time

A typical DPSF run might consist of 3 solutions to the boundary value problem, and two wake alignments, followed by a force calculation. For a 4-bladed propeller with 153 control points, this takes 5.2 minutes on an IBM 4381 or 18.2 minutes on a DEC Micro VAX II.

6. CONCLUSIONS AND RECOMMENDATIONS

The Ducted Propeller in Steady Flow (DPSF) analysis program is a useful tool in designing both ducted and banded propellers. The test runs which have been made have shown good agreement with published thrust and torque data in the case of a banded propeller, and good total thrust predictions in the case of a ducted propeller, although the predictions of duct thrust and shaft torque in the latter case differed significantly from measured values. The solution appears to converge quite quickly with increasing panel density for all force predictions except for duct thrust.

The representation of tip clearance in DPSF is by 1) defining the equivalent "inviscid gap" which results in the same volume of leakage flow as the physical gap, and 2) placing the outermost blade chordwise vortex in the optimum position so as to speed numerical convergence with respect to spanwise panel density. This approach appears to be satisfactory for a "global" solution, including the prediction of propeller forces. The detailed prediction of flow through the gap, including the effect of the duct boundary layer, could presumably be accomplished using a finite element method, using the predicted blade tip loadings from DPSF as input.

Additional work which would improve the accuracy and usefulness of DPSF are:

- 1) The development of a field point velocity program to aid in the design of struts, stators, etc.
- 2) The development of a cavitation prediction capability using the results of this field point velocity program.
- 3) The inclusion of the propeller hub in the boundary value problem. This is made relatively easy by the modular nature of DPSF.
- 4) The non-linear representation of the propeller duct. A typical duct thickness/chord ratio is 15%, large enough that improvements could be made by placing the singularities on the duct surface rather than the mean line.
- 5) More comparisons between DPSF predictions with experimental data. The comparisons made so far are quite limited, using data obtained at fairly low Reynolds numbers. More recent data is necessary to critically evaluate the accuracy of the program.
- 6) More experimental work in the area of determining the nature of flow through small gaps.
- 7) The development of a local tip gap solution which

could be run iteratively with DPSF to predict the exact nature of the flow in the gap, including the occurrence and extent of gap cavitation, while refining the prediction of global performance characteristics.

7. REFERENCES

Booth, T.C., P.R. Dodge and H.K. Hepworth (1981), "Rotor-Tip Leakage Part 1 - Basic Methodology," *Journal of Engineering for Power, ASME Paper No. 81-GT-71.*

Durand, W.F. (1963), *Aerodynamic Theory*, Dover, New York.

Gearhart, W.S. (1966), "Tip Clearance Cavitation in Shrouded Underwater Propulsors," *Journal of Aircraft, Vol. 3, No. 2.*

Greeley, D.S. (1982), "Marine Propeller Blade Tip Flows," *MIT Dept. of Ocean Engineering Report No. 82-3.*

Greeley, D.S. and J.E. Kerwin (1982), "Numerical Methods for Propeller Design and Analysis in Steady Flow," *Transactions SNAME, New York.*

Hoerner, S.F. (1965), *Fluid Dynamic Drag*, Hoerner Fluid Dynamics, Brick Town, N.J.

Hoerner, S.F. and H.V. Borst (1975), *Fluid Dynamic Lift*, Hoerner Fluid Dynamics, Brick Town N.J.

James, R.M. (1972), "On The Remarkable Accuracy of the Vortex Lattice Method," *Computer Methods in Applied Mechanics and Engineering, Vol. 1.*

Kerwin, J.E. and C-S Lee (1978), "Prediction of Steady and Unsteady Marine Propeller Performance by Numerical Lifting-Surface Theory," *Transactions SNAME, New York.*

Kerwin, J.E., P. Mandel and S.D. Lewis (1972), "An Experimental Study of a Series of Flapped Rudders," *Journal of Ship Research, Vol. 16, No. 4.*

Lan, C.E. (1974), "A Quasi--Vortex-Lattice Method in Thin Wing Theory," *Journal of Aircraft, Vol. 11, No. 9.*

Shalnev, K.K. (1958), "Cavitation in Turbomachines," *Water Power, January, 1958.*

van Gunsteren, L.A. (1970), "Ring Propellers and Their Combination with a Stator," *Marine Technology, Vol. 7, No. 4.*

Van Houten, R.J. (1983), "Analysis of Banded Propellers

in Steady Flow," MIT Dept. of Ocean Engineering
Report No. 83-13.

van Manen, J.D. (1962), "Effects of Radial Load Distribution
on the Performance of Shrouded Propellers,"
Transactions of the Royal Institution of Naval
Architects.

Wadia, A.R. and T.C. Booth (1981), "Rotor-Tip Leakage:
Part II - Design Optimization Through Viscous
Analysis and Experiment", ASME Paper No. 81-GT-72.

APPENDIX A. MAGNITUDE OF THE GAP BOUNDARY LAYER THICKNESS.

The nature of the flow in the clearance gap of a ducted propeller can be found by considering the relative thickness of the viscous boundary layer within the gap. This boundary layer is that due to the pressure-driven flow through the gap rather than the boundary layer on the inner surface of the duct. If one assumes laminar flow, the ratio of the displacement thickness to the clearance gap is given by

$$\frac{\delta^*}{h} \approx \frac{\sqrt{vt/U_g}}{h}$$

where δ^* is the displacement thickness, h is the clearance gap, t is the blade thickness, U_g is the velocity in the gap, and v is the kinematic viscosity. From Bernoulli's equation, one finds that

$$U_g = \sqrt{2 \Delta p / \rho}$$

where ρ is the density and Δp is the pressure difference across the blade tip. Δp can be obtained from the blade lift coefficient near the tip:

$$\Delta p = C_L \cdot \frac{1}{2} \rho U_{tip}^2$$

where U_{tip} is the relative inflow velocity at the blade tip.

Combining the above equations, one obtains the following:

$$\frac{\delta^*}{h} = \left[\frac{v t / h}{h U_{tip} \sqrt{C_L}} \right]^{\frac{1}{2}}$$

A typical full scale propeller might have the following characteristics:

$$t/h=10 \quad h=.02 \text{ ft} \quad U_{\text{tip}}=150 \text{ fps} \quad C_L=.2$$

So that $\delta^*/h \approx .009$, indicating that the flow is primarily inviscid.

Assuming that tip speed scales with the square root of the length scale λ , δ^*/h scales as $\lambda^{-.75}$, so that a 1/20 scale model of the above propeller would have a relative boundary layer thickness of $\delta^*/h \approx .09$. So even at this scale ratio, inertial effects will dominate.

In the case of an incoming shear flow due to a duct boundary layer, these considerations still apply. The existence of such a boundary layer is certainly due to viscous effects, but the local gap flow will be primarily an inviscid interaction between the shear flow and the local pressure field.